



HAL
open science

Morphology and sedimentary architecture of a modern volcanoclastic turbidite system: The Cilaos fan, offshore La Réunion Island

Emmanuelle Sisavath, Nathalie Babonneau, Francky Saint-Ange, Patrick Bachèlery, Stéphane Jorry, Christine Deplus, Béatrice de Voogd, Bruno Savoye

► To cite this version:

Emmanuelle Sisavath, Nathalie Babonneau, Francky Saint-Ange, Patrick Bachèlery, Stéphane Jorry, et al.. Morphology and sedimentary architecture of a modern volcanoclastic turbidite system: The Cilaos fan, offshore La Réunion Island. *Marine Geology*, 2011, 288 (1-4), pp.1-17. 10.1016/j.margeo.2011.06.011 . insu-00656017

HAL Id: insu-00656017

<https://insu.hal.science/insu-00656017>

Submitted on 10 Jan 2012

HAL is a multi-disciplinary open access archive for the deposit and dissemination of scientific research documents, whether they are published or not. The documents may come from teaching and research institutions in France or abroad, or from public or private research centers.

L'archive ouverte pluridisciplinaire **HAL**, est destinée au dépôt et à la diffusion de documents scientifiques de niveau recherche, publiés ou non, émanant des établissements d'enseignement et de recherche français ou étrangers, des laboratoires publics ou privés.

1 **Morphology and sedimentary architecture of a modern volcanoclastic** 2 **turbidite system: The Cilaos fan, offshore La Réunion Island**

3 Emmanuelle Sisavath^{1&2*}, Nathalie Babonneau³, Francky Saint-Ange⁴, Patrick Bachèlery¹,
4 Stephan J. Jorry², Christine Deplus⁵, Béatrice De Voogd⁶, Bruno Savoye^{2†}.

5
6 1 : Laboratoire GéoSciences Réunion, Université de la Réunion, Institut de Physique du Globe de Paris CNRS,
7 UMR7154, 15 avenue René Cassin, BP 7151. 97715 Saint Denis messag Cedex 9. La Réunion.

8 2 : IFREMER, Géosciences Marines, Laboratoire Environnements Sédimentaires, BP70, 29280 Plouzané,
9 France.

10 3 : Université de Brest, IUEM, UMR CNRS 6538, Brest, France

11 4 : Geological Survey of Canada (Atlantic), Bedford Institute of Oceanography, P.O. Box 1006, Dartmouth,
12 Nova Scotia, B2Y 4A2, Canada

13 5 : Institut de Physique du Globe de Paris et CNRS, UMR 7154, 1, rue Jussieu, 75238 Paris Cedex 05, France

14 6 : Université de Pau et des pays de l'Adour CNRS, UMR 5212, , 64000 Pau, France

15

16 † Deceased on August 2008, the 21th

17 * corresponding author: Ph : +33.2.29.00.85.65 ; Fax : +33.2.98.22.45.70 ; email :

18 emmanuelle.sisavath@ifremer.fr

19

20 **Abstract**

21 Recent oceanographic surveys revealed the existence of five volcanoclastic deep-sea fans off
22 La Réunion Island. The Cilaos fan is a large volcanoclastic submarine fan, connected to rivers
23 that episodically experience torrential floods through a narrow and steep shelf-slope system.
24 New piston cores presented in this study together with echosounder profiles give new insight
25 into the evolution of this extensive and sand-rich turbidite system. The Cilaos fan extends
26 over 15,000 km² on an abyssal plain and is compartmentalized by topographic highs. Located
27 southwest of the island, the sedimentary system consists of a canyon area and a deep sea fan
28 divided into a proximal and a distal fan. The proximal fan is characterized by its wide extent
29 and coarse-grained turbidites. The distal fan is characterized by elongated structures and fine-
30 grained turbidites. A detailed morphological study of the fan which includes the analysis of
31 swath bathymetry, backscatter, echosounder, and piston core data shows that the Cilaos fan is
32 a complex volcanoclastic deep-sea fan, highly influenced by preexisting seafloor irregularities.
33 The canyons and the slope area show a complex and evolving sediment feeding system with a
34 direct sediment input by the river and irregular sediment supply by submarine landslide.
35 Three main construction stages are identified for this system: (1) an old incision phase of the
36 channels forming wide turbidites extending over the entire distal fan; (2) a period of no or low

37 activity characterized by a thick layer of hemipelagic mud; and (3) a local reactivation of the
38 channel in the proximal fan. Each stage seems to be linked to a different sediment source with
39 a progressively increasing contribution of hemipelagic sediment and mud in younger stages.

40

41 **1. Introduction**

42 Volcanic islands are subject to numerous studies on their construction or structural evolution
43 as well as their eruptive activity, but few studies focus on the submarine part of these edifices.
44 The knowledge of processes affecting the submarine slope of these volcanoes including the
45 surrounding basin is an essential step for a better understanding of sediment transfer toward
46 the seafloor, and to constrain the overall evolution of these geodynamic systems.

47 Mass wasting processes are an inherent part of volcanic islands with specific characteristics
48 depending on the geodynamic setting, the sediment supply, slope angle, and climate. They are
49 now largely considered as a major process in the evolution of such islands, significantly
50 contributing to the edification of submarine slopes (Deplus et al., 2001; Le Friant et al., 2004;
51 Masson et al., 2002; Moore et al., 1989; Oehler et al., 2008). Increase in resolution of marine
52 geophysical data (swath bathymetry, echosounder and seismic data) have contributed to
53 improve our knowledge of volcanoclastic systems at the base of volcanic slopes (Bosman et
54 al., 2009; Casalbore et al., 2010; Deplus et al., 2001, 2009) and to document the occurrence of
55 several gravity related processes, including turbidite systems.

56 Recent oceanographic cruises over submarine flanks of La Réunion Island and the
57 surrounding oceanic plate led to the discovery of several volcanoclastic turbidite systems
58 extending to more than 200 km from the island (Saint-Ange, 2009; Sisavath et al., 2009). The
59 existence of volcanoclastic turbidite off a volcanic island is not specific to La Réunion Island.
60 Other examples are Hawaii (Garcia and Hull, 1994) and Canary Islands (Acosta et al., 2003)
61 where volcanoclastic turbidite are visible more than 400 km from these islands. Volcanoclastic
62 systems in a subduction context can also be considered such as Stromboli Island (Romagnoli
63 et al., 2009) and Lesser Antilles Arc (Deplus et al., 2001; le Friant et al., 2009) where recent
64 studies showed detailed morphology of the submarine slopes. All these systems are located in
65 deep marine sedimentary basins surrounded volcanic islands. They show morphological
66 structures like canyons, channels or sediment-waves (Casalbore et al., 2010; Wynn et al.,
67 2000), but no extensive channel lobe systems are observed, as in offshore La Réunion Island-

68 No study has yet assessed a whole modern turbidite volcanoclastic system, however such a
69 study would include a detailed examination of the sedimentary architecture and
70 characterization of the sediment source. Our paper focuses on the study of the largest
71 volcanoclastic turbidite system around La Réunion Island: the Cilaos deep-sea fan, located
72 southwest of the island. It is the first documented example of a very extensive fan (with
73 channel and lobes) originating from a volcanic island. The Cilaos turbidite system, was first
74 described by Saint-Ange et al. (2011) and the new high-resolution dataset (swath-bathymetry
75 backscatter and echosounder data) and sediment cores presented in this paper illustrate a
76 complex organization of sedimentary bodies and structures from the canyon to the distal part
77 of the turbidite fan.

78 This study not only provides an opportunity to investigate a modern volcanoclastic turbidite
79 system but also to study the sedimentary processes which are involved in the development of
80 this type of depositional deep-sea system. A large data set was examined in order to do a
81 detailed investigation of seafloor morphology, superficial sediment distribution and recent
82 evolution of the Cilaos deep-sea fan.

83 **2. Regional setting**

84 **2.1. Geological setting of La Réunion**

85 La Réunion Island is the emerged part of an intraplate volcanic system located in the western
86 part of the Indian Ocean (21°S, 55°E), about 750 km east of Madagascar (Fig. 1). La Réunion
87 is commonly considered as the recent expression of the hotspot which formed the Deccan
88 Traps (65 Ma ago) and subsequently the Mascarene Plateau and Mauritius Island (Bonneville
89 et al., 1988; Duncan et al., 1989; Morgan, 1981). It could be one of the seven (or ten) main
90 deep mantle plumes on Earth (Courtillet et al., 2003). La Réunion Island is located in the
91 Mascarene Basin, on a compartment of oceanic lithosphere bordered by two fracture zones
92 (FZ) separated by 350 km: the Mahanoro FZ to the west and Mauritius FZ to the east (Fig. 1).

93 The subaerial island accounts for only three percent of the whole edifice (De Voogd et al.,
94 1999), and reaches a height of 3070 m above sea level. The submerged base of the volcanic
95 edifice is 4,200 meters below sea level (mbsl), such that the total relief of the edifice is ~7
96 km. The morphology of the island is dominated by two basaltic shield-volcanoes. The Piton
97 des Neiges volcano occupies the northwestern part of the island (Fig. 1). It started to grow
98 during the Pliocene, more than 2.1 Ma ago, and has been inactive in the last 0.012 Ma (Deniel
99 et al., 1992; McDougall, 1971; Quidelleur et al., 2010). The main and most original feature of

100 Piton des Neiges is the existence of three major erosional depressions, called “cirques”,
101 opened in the center of the volcano (Fig. 1). The “cirques” are partly filled by unconsolidated
102 detritic rocks like volcanic debris avalanche deposits, debris flow deposits and other breccia
103 (Arnaud, 2005; Bret et al., 2003; Fèvre, 2005; Oehler et al., 2005). The Piton de la Fournaise
104 volcano (2632 m high) is a highly active volcanic shield. Activity at Piton de la Fournaise
105 started less than 0.6 Ma ago (Gillot and Nativel, 1989). Eruptive activity is mainly composed
106 of basaltic lava flows and fountains, or moderate rhythmic explosions at the vent. More
107 explosive activity is rare, typically associated with phreatic or phreatomagmatic eruptions
108 generated at the Dolomieu summit crater or near the coast. The frequent historic volcanic
109 activity of Piton de la Fournaise is described by Bachelery et al. (1983), Lenat et al. (2009),
110 Michon and Saint-Ange (2008), Peltier et al. (2008, 2009) and Stieltjes and Moutou (1988).

111 The existence of an older and largely dismantled edifice, Les Alizés volcano, predating Piton
112 de la Fournaise volcano, is proposed from geophysical studies (Gailler et al., 2009;
113 Malengreau et al., 1999; Rousset et al., 1989) and drill hole data (Rancon et al., 1989). An age
114 of 3.3 Ma was recently obtained on a sample dredged on the NE flank of Piton de la
115 Fournaise (Smietana et al., 2010).

116 Four submarine bulges were described to the east, north, west, and south submarine flanks of
117 La Réunion Island. Lénat and Labazuy (1990) then Oehler et al (2004) propose that the
118 submarine flanks of La Réunion Island are mostly built by accumulation of debris avalanche
119 deposits: the superposition and/or juxtaposition of such deposits leading to the formation of
120 the bulges. A recent study (Le Friant et al., 2011) proposed that the chaotic deposits on the
121 submarine flanks of Piton des Neiges come from slow deformations such as sliding or
122 spreading, rather than flank collapse. These slow processes lead to secondary submarine slope
123 instability and in some cases they have triggered unconfined turbidity flows (Le Friant et al.
124 2011). A study of the recent submarine sedimentation off Piton de la Fournaise Volcano
125 revealed coarse-grained turbidites and sandy lobes, confirming the presence of turbidity
126 currents (Ollier et al., 1998).

127 **2.2. Hydrogeological settings and climate**

128 La Réunion Island is located in the subtropical zone where the climate is characterized by two
129 seasons: a hot and wet season during the austral summer; and a cooler and dryer season
130 during the austral winter. Trade winds from the east induce highly variable precipitation
131 regimes in time and space, with a wet windward side (east) and a dry leeward side (west).
132 Rainfalls also vary according to elevation, with a maximum rainfall at mid-slope. Rainfall

133 intensities are high with up to 1825 mm for daily precipitation amounts and up to 12,000 mm
134 for yearly precipitation amounts (Barcelo et al., 1997; Robert, 2001).

135 On La Réunion, high erosion rates are caused by the wet tropical climate and are amplified by
136 seasonal cyclonic conditions (Louvat and Allegre, 1997; Rad et al., 2007). Hurricanes induce
137 rainfalls and torrential floods, causing land erosion and highly concentrated sediment loads in
138 the main river mouths (Bret et al., 2003; Fèvre, 2005; Garcin et al., 2005; Saint-Ange, 2009).

139 Recent studies (Louvat and Allegre, 1997) underline the particularities of the erosion of
140 basaltic terrains: incision rates are close to those estimated in active orogenic areas, with
141 values ranging between $0.47 - 3.4 \text{ m.kyr}^{-1}$ for La Réunion Island. These high erosion rates
142 result in a dense hydrographic network with more than 750 gullies and rivers on the island,
143 only twenty of them are perennial. Five main rivers incise the slopes of the volcanoes creating
144 deep valleys (Fig. 1).

145 The transition between the subaerial and the submarine environments is characterized by a
146 narrow shelf that is locally absent especially around the Piton de la Fournaise (Fig. 2). The
147 local absence of the shelf and the presence of steep submarine slopes around the island favour
148 a rapid transfer of sediment from the coast toward the submarine slopes of the volcanic
149 edifice and on to the abyssal plain.

150 One of the major rivers of the Island is the Rivière Saint-Etienne, whose headwaters reach
151 altitudes of 3000 m (Fig. 1). The Rivière Saint-Etienne has a drainage basin of about 360 km^2
152 (Figs. 1 and 2) composed of two main tributaries: the “Bras de Cilaos” and the “Bras de la
153 plaine”. The “Bras de Cilaos” drains the inner part of the cirque while the “Bras de la Plaine”
154 comes from the outer slopes of the cirque. They merge 6 km from the coast to form the
155 Rivière Saint-Etienne. The basement lithology in the drainage basin is dominated by coarse-
156 grained sediments ranging from sand to boulders (Saint-Ange et al, 2011). The mean fluvial
157 solid load of the Rivière Saint-Etienne is estimated around $470\,000 \text{ m}^3/\text{yr}$ and during
158 important floods it reaches $1\text{-}2 \text{ million m}^3/\text{yr}$ (SOGREAH, 1998).

159 **3. Data and methods**

160 The dataset used in this paper was collected during the recent oceanographic cruises
161 FOREVER in April 2006 onboard the RV *L'Atalante*, ERODER 1 in July 2006 onboard the
162 BHO *Beautemps-Beaupré*, and ERODER 2 in January 2008 onboard the RV *Meteor* (Fig.
163 2A).

164 During the FOREVER survey, the lower submarine slopes of La Réunion volcanic edifice
165 and the surrounding oceanic plate were imaged using a hull-mounted Simrad EM12 Dual
166 multibeam echo-sounder system (frequency 12 kHz, 162 beams with $1.8^{\circ} \times 3.5^{\circ}$ angular
167 resolution, Fig. 2A). The coverage extends from the fracture zones to 300 km south of the
168 island. 3.5 kHz echosounder and seismic reflection data were acquired along 12,200 km of
169 profiles. Two Kullenberg piston cores were also successfully collected in the Cilaos deep-sea
170 fan.

171 Cruise ERODER 1 (Fig. 2A) complemented the preexisting swath bathymetry and backscatter
172 data on the upper submarine slopes of the volcanic edifice. It aimed to establish the link
173 between the onshore morphological structures and the deep-marine morphology. Data were
174 collected using a hull-mounted Kongsberg Simrad EM120 system (frequency 12 kHz, 192
175 beams with $1^{\circ} \times 1^{\circ}$ angular resolution). Two Kullenberg piston cores were successfully
176 collected in the study area.

177 Cruise ERODER 2 (Fig. 2A) was mainly devoted to coring the sedimentary systems. Twelve
178 piston cores, with a diameter of 125 mm, were collected using a Kullenberg type piston corer.
179 A total of eight cores are located in the Cilaos deep-sea fan. In addition, more detailed swath
180 bathymetry and backscatter data (Kongsberg Simrad EM120 system) and echosounder data
181 (Parasound system) were collected over the Cilaos fan. The coverage was also extended
182 further south.

183 Results shown in this paper are mainly based on the analysis of swath bathymetry, backscatter
184 data, Parasound and 3.5 kHz echosounder profiles, and sedimentological study of piston
185 cores. The bathymetry and the sonar backscatter image of cruises ERODER 1 and ERODER2
186 were processed at IFREMER with Caraïbes software (developed by IFREMER). Sound speed
187 of 1600 m/s has been applied for the time to depth conversion.

188 The submarine surface of Cilaos fan was characterized on the backscatter imagery by acoustic
189 facies ranging from dark (high reflectivity) to light grey (low reflectivity). Five main types of
190 sediment acoustic facies were identified on the echosounder profiles: (1) a hyperbolic unit
191 with irregular hyperboles; (2) a continuous stratified unit characterized by parallel and
192 continuous reflectors; (3) a semi-transparent unit corresponding to a thin surface echo without
193 internal reflectors; (4) a discontinuous stratified unit characterized by stratified echofacies
194 with discontinuous reflectors; and (5) a non-penetrative unit corresponding to a strong and
195 prolonged surface echo.

196 A total of thirteen cores were collected and analyzed on the Cilaos turbidite system (Table 1
197 and Fig. 2A): one was collected in the canyon area (KERO-18); three cores were located in
198 the upper part of the fan (KERO-01, KERO-02 and KERO-11); six cores were collected from
199 the western part of the fan (FOR-C2, KERO-09, KERO-12, KERO-13, KERO-14 and KERO-
200 15); and three cores were retrieved in the central part of the fan (FOR-C1, KERO-16, and
201 KERO-17). Sedimentary descriptions were done for all the cores, with a particular emphasis
202 on sediment color, visual grain size and turbidite/hemipelagite/pelagite differentiation. A
203 series of 1-cm-thick sediment slabs were collected for each split core section for X-
204 radiography using a digital X-ray imaging system SCOPIX (Migeon et al., 1999). Digital
205 images were acquired to provide a precise identification of the sedimentary structures.
206 Sediment cores were sampled for grain-size analyses using a Coulter laser micro-
207 granulometer (LS130).

208 In this paper, we used eight cores showing the most representative sedimentary facies of the
209 thirteen cores (Table 1, names in bold and Fig. 3). One core is located in the canyon area
210 (KERO-18), two cores are located in the upper part of the fan (KERO-01 and KERO-11), two
211 cores are in the central part (KERO-16 and KERO-17) and three in the western part (KERO-
212 09, KERO-13 and KERO-15). These cores are located on and correlated with the echosounder
213 profiles.

214 Four AMS dates were also obtained, two on core KERO-09 and two on core KERO-16. For
215 each measurement, about 500 specimens of *Glogigenrinoides ruber* and *Glogigerinoides*
216 *sacculifer* were picked from the >150 mm fraction. These aliquots were analyzed at the
217 Poznan Radiocarbon Lab., Poland, and at the “Laboratoire de Mesure du Carbone 14” at
218 Sarclay. Reported radiocarbon ages have been corrected for a marine reservoir effect of 400
219 years and converted to calendar years using CALIB Rev 6.0 (Reimer and Reimer, 2001).
220 Calibrated kilo years before present will be referred as ka.

221 **4. Results**

222 **4.1. Five volcanoclastic deep-sea fans off La Réunion Island**

223 The new dataset led to the discovery of five volcanoclastic deep-sea fans showing
224 morphological structures typical of a turbidite system like, canyon, channel and sediment
225 waves (Fig. 2B). They show low reflectivity and display complex geometries, directly
226 constrained by the seafloor morphology. On land, they are related to major erosional features,
227 which constitute the main drainage area of the island. In each case, submarine canyons are
228 directly connected to the main river mouths (Figs. 1 and 2B).

229 The Mafate fan (Fig. 2B, 1) is connected to the Cirque of Mafate and coalesces with the
230 Saint-Denis fan (Fig. 2B, 2), which is continuous with the Rivière Saint-Denis. The Salazie
231 fan (Fig. 2B, 3) derives from multiple sources and is connected to the Cirque of Salazie. The
232 Saint-Joseph fan (Fig. 2B, 4) is the only system connected to the Piton de la Fournaise
233 volcano, and considered to be a fan in an embryonic stage. We focus in this paper on the
234 Cilaos fan (Fig. 2B) which is a wide fan connected to the Cirque of Cilaos through the Rivière
235 Saint-Etienne.

236 The relationship between the activity of these turbidite systems and the largest hurricanes is
237 not completely established but observations of flood impact on land (erosion and transport
238 volume) suggest a direct sediment transfer toward the canyon head during extreme floods.

239 Volcanic and sedimentary features mainly shape the ocean floor on the abyssal plain (Deplus
240 et al. 2007; Deplus et al., 2009). Volcanic features consist of a series of elongated ridges
241 (named R1 to R4 on Fig. 3B) which display high reflectivity, and include several elongated
242 volcanic structures and isolated seamounts. In the southwestern part of the fan, linear features
243 with high reflectivity are parallel to the Mahanoro fracture zone (Fig. 3). They probably
244 correspond to small fracture zones associated with the offset of the fossil axis to the south.
245 Other topographic highs are visible in the bathymetry and have a low reflectivity contrast
246 (brown areas in Fig. 3B). They correspond to sedimentary accumulations on volcanic highs,
247 like the large ridge named SR at the south of La Réunion (Deplus et al. 2007; Deplus et al.,
248 2009).

249 **4.2. Morphology and superficial structure of the Cilaos deep-sea fan**

250 The Cilaos deep-sea fan is the largest volcanoclastic turbidite system off La Réunion Island.
251 On the backscatter image, the Cilaos fan corresponds to a wide area with low reflectivity (Fig.
252 3A). The whole turbidite system is more than 300 km long and covers an area of about 15,000
253 km². Located southwest of the island, this sedimentary system consists of two main parts: a
254 canyon area (Fig. 3B, in blue) starting at the coast, directly fed by the recurrent flash floods of
255 the Rivière Saint-Etienne; and a deep-sea fan that develops at about 4500 m of water depth on
256 the abyssal plain (Saint-Ange, 2009; Saint-Ange et al., 2011). The deep-sea fan was initially
257 laterally divided into three main areas: the western, the central, and the eastern parts separated
258 by two NE-SW sub-parallel volcanic ridges called R1 and R2 (Fig. 3) (Saint-Ange, 2009).
259 Advancements in understanding due to new data presented in this paper enable further
260 subdivision of the system into: (1) The proximal fan (Fig. 3B, in red) corresponding to a wide

261 area with a low reflectivity; and (2) the distal fan (Fig. 3B, in yellow) which is characterized
262 by elongated structures that are developed between volcanic ridges.

263 **4.2.1. The Cilaos canyons**

264 Canyons directly incise the chaotic deposits that form the submarine flanks of the volcanic
265 edifice (Fig. 4) (Lenat and Labazuy, 1990; Oehler et al., 2008). They are 70 km long and their
266 slopes decrease from 8° at shallow depth to less than 1° dip near the base of the volcanic
267 edifice (Fig. 5).

268 Two wide rectilinear canyons make up the valley area: the Saint-Etienne and the Pierrefonds
269 canyons (Fig. 4B). For each of them, the incision is about 100 m deep. The Pierrefonds
270 canyon is located in front of the paleo-river outlet of the Rivière Saint-Etienne and is
271 connected to the shelf by many tributaries (Fig. 4C). This canyon is well developed and
272 characterized by high reflectivity on the backscatter image and by a smooth surface on the
273 bathymetric map. It is a flat-bottomed canyon 3 km wide and 30 km long. Some
274 morphological highs (possible relicts of the chaotic deposits) are visible in the canyon path,
275 inducing local divergences and forming a braided system (Fig. 4A).

276 The Saint-Etienne canyon is 4 km wide and seems to be directly connected with the Rivière
277 Saint-Etienne (Fig. 4B). On its western side, limited by the “Etang-Salé” volcanic ridge, it
278 also receives several tributary canyons from a shelf-upper slope sector (Fig. 4). The canyon is
279 partitioned in two distinct areas, the upper and the lower canyon. The upper Saint-Etienne
280 canyon begins at 300 m water depth and extends to the southern extremity of the “Etang-
281 Salé” volcanic ridge at depth of 2200 m (Fig. 4A). It has a smooth morphology and is
282 characterized by high reflectivity on the backscatter image.

283 The lower canyon has a rougher morphology on the bathymetry and a mottled appearance on
284 the backscatter image (Figs. 4A and 4B). The chaotic floor of the lower canyon is cut by a
285 narrow incision located in the prolongation of the upper Saint-Etienne canyon (Fig. 4). This
286 incision is 20 m deep and 13 km long.

287 North of the Saint-Etienne and Pierrefonds canyons and north of the “Etang-Salé” ridge, a
288 wide valley is visible. It is a wide trough (about 10 km wide) with a rough floor and a low
289 reflectivity on the backscatter image named the North Valley (Fig. 4A). A set of gullies (Fig.
290 4C, yellow dash line) named the North Gullies, cut this valley and join the incision of the
291 lower Saint-Etienne canyon. The North Gullies were connected to the hydrographic network
292 onland (Fig. 4C). These gullies present a rough floor characterized by a mottled facies on the

293 backscatter image (Fig. 4B). Local undulations are visible on their western side on the shaded
294 relief map (Fig. 4C and Fig. 6). These undulations are developed in a water depth of about
295 2000 m. Their geometry varies from symmetrical with a crest in the midslope to asymmetrical
296 at the upslope. Their amplitude ranges from 5 to 30 m and their wavelength varies from 500
297 to 700 m (Fig. 6). The slope gradient is 2.5° . They display similar characteristics to the
298 coarse-grained sediment waves observed on the submarine slopes of the western Canary
299 Islands (Wynn et al, 2000), except for height, which is much greater at La Réunion.
300 Downslope, the North Valley and the two main canyons merge into a single canyon, the
301 Cilaos canyon (Fig. 4) (Saint-Ange, 2009). At the base of slope, the Cilaos canyon (10 km
302 wide) divides into many narrow channels that feed the Cilaos deep-sea fan (Fig. 7).

303 **4.2.2. The Proximal Fan**

304 The proximal fan is characterized by a low reflectivity and a wide extent with a maximum
305 width of 120 km (Figs. 3 and 7). It extends from a depth of 3800 to 4300 mbsl, with gradients
306 ranging from 1.5° to 0.1° (Fig. 5). Only few sedimentary structures (channels, lobate
307 structures, sediment waves), mainly located on the western side of the turbidite system, are
308 visible at the surface of the proximal fan (Fig. 7).

309 A main field of sediment waves (Figs. 6 and 7) is located in the channel, at the slope break
310 close to the transition between the canyon and the fan (Fig. 5) at a water depth of 3500-4000
311 m. These features are particularly highlighted by a contrast in backscatter (Figs. 6 and 7). The
312 crest orientation of the sediment waves is perpendicular to the Cilaos valley axis. Their
313 amplitude is more than 10 m and their wavelength increases downslope from 1 km to 3 km
314 (Fig. 6).

315 At the base of slope, the proximal fan spreads over the abyssal plain. Its morphology is
316 controlled by the presence of bathymetric highs (often with high reflectivity), which
317 correspond to relief caused by volcanic and sedimentary structures (Fig. 7).

318 Narrow channels coming from the canyon area mainly develop in the western part of the
319 proximal fan. They form a braided system composed of elongated bodies. This system is
320 bordered by a small field of sediment wave that show the same characteristics as the main
321 sediment waves field (Fig. 7). These bodies are probably small lobes with discontinuous
322 contours. Some narrow channels of the canyon area also extend in the eastern part of the
323 proximal fan but they quickly disappear. They open onto the abyssal plain forming elongated

324 bodies with low backscatter reflectivity, comparable to those observed in the western part
325 (Fig. 7).

326 On echosounder profiles, chaotic deposits are characterized by an irregular hyperbolic facies
327 (Fig. 8, profile FOR-18). They are slightly incised by small channels in the upper part. Further
328 downslope (Fig. 8, profile FOR-9) the irregular hyperbolic facies changes into a continuously
329 stratified unit, more visible on the western side. On figure 9, the detailed interpretation of 3.5
330 kHz echosounder profiles shows a vertical succession of three units: U1, U2, and U3. Unit U1
331 (Fig. 9) corresponds to the lowest imaged unit. Stronger reflectors, indicating a high
332 impedance contrast, mark its upper limit. Reflectors are continuous and moderate to high
333 amplitude. Unit U2 (Fig. 9) overlies unit U1 and is semi-transparent (low amplitude). It is
334 thinner than 6 m and covers the whole distal fan. This transparent unit U2 is mostly covered
335 locally by another stratified unit U3 (Fig. 9). This youngest stratified unit U3 overlies the
336 whole proximal fan. Its thickness decreases distally from the base of slope.

337 **4.2.3. The Distal Fan**

338 The distal turbidite system comprises western and central parts of the Cilaos fan. It is
339 characterized by elongated structures with low reflectivity, corresponding to narrow channels
340 continuing from the proximal fan (Fig. 10). The reflectivity is low in the channel floors (Fig.
341 10). It extends from a depth of 4300 to 4500 mbsl, with gradients less than 0.1° (Fig. 5).

342 A deeply incised and rectilinear channel characterizes the western part of the distal fan. In the
343 upper part, the incision is lower than 10 m deep and about 1.5 km wide. Area of higher relief
344 covered by sediment accumulations divide this main channel into three minor channels
345 (incisions about 10 m deep) converging westward into a unique, WNW-ESE oriented channel
346 (Fig. 10). This is a highly incised (30 m deep) and long channel (75 km). Its western edge is
347 halted by volcanic highs and it abruptly turns to the southwest (Fig. 10).

348 The central part of the distal fan is composed of a rectilinear channel showing a NE-SW
349 orientation with an incision depth of about 15 m that increases downslope (Fig. 10). The
350 volcanic ridges seem to directly control the channel direction. To the south, the channel in the
351 central part of the distal fan joins the same WNW-ESE oriented channel from the western part
352 of the fan (Fig. 10). This WNW-ESE oriented channel starts somewhere upstream of these
353 confluences, but it disappears in the eastern part. No structures are visible on the bathymetry
354 and the backscatter image (Fig. 10).

355 The Cilaos turbidite system ends in a small fracture zone associated to the offset of the
356 Mahanoro fracture zone, where no depositional structures of the distal fan are visible (Fig.
357 10).

358 On echosounder profiles, the distal fan is characterized by the presence of units U1 and U2
359 over the whole area (Figs. 8 and 9). Unit U3 covers most of the eastern and central parts of
360 the distal fan. In the western distal part, channels are observed. While moving away from the
361 island the U-shaped valley, visible on profile FOR-13 (Fig. 8), has evolved into narrow V-
362 shaped valleys with non-penetrative echofacies in the channel floors as visible on profiles
363 FOR-45 and ERO2-07 (Fig. 8). In the central part, a wide shallow U-shaped valley has
364 developed. The width of this channel decreases from 4 km on profiles FOR-11 and FOR-13
365 (Fig. 8) to 1 km on profile ERO2-07 (Fig. 8). The channel floor passes from continuous
366 (profile FOR-13, Figs. 6 and 8B) to discontinuous (profile FOR-45, Figs. 8 and 9) stratified
367 units with superficial high-amplitude reflectors. The eastern part is characterized by
368 continuous bedded facies with few channelized structures that are only visible on profiles
369 FOR-45 and ERO2-07 (Fig. 8). A small field of sediment waves is visible on profile FOR-13
370 (Figs. 6 and 8) located on an overbank. Their geometry is asymmetrical. They have an
371 amplitude of 4 to 6 m, a wavelength of about 700 to 850 m (Fig. 6 and their slope gradient is
372 0.2°. They display similar characteristics to the coarse-grained sediment waves observed on
373 the submarine slopes of the western Canary Islands (Wynn et al, 2000).

374 No typical turbidite levee structure can be identified in the distal fan on the channel sides in
375 the 3.5 kHz profiles. Only a few features suggest levee structures in the distal part of the fan
376 which are visible on profiles FOR-45, ERO2-07, FOR-4a, and FOR-4b (Fig. 8).

377 **4.3. Sedimentary Facies**

378 Cores retrieved in the Cilaos fan are mainly composed of brown clay, silt and sand. The silty
379 and sandy layers are characterized by a dark color due to the dominance of volcanoclastic
380 elements (Fig. 11). Glass shards, angular olivine, pyroxene, oxides and feldspar crystals,
381 bioclasts and rock fragments are the main petrographic components of these sands.

382

383 **4.3.1. Sedimentary facies in the canyon area and the proximal fan**

384 The three cores KERO-18, collected in the canyon area, and KERO-01 and KERO-11
385 collected on the proximal fan, best illustrate the sedimentation in the canyon area and the
386 proximal fan. Core KERO-18 is located in the Saint-Etienne canyon about 15 km from the

387 shoreline at 2056 m water depth. It recovered the only samples (about 30 cm) of coarse-
388 grained sand and gravel (Fig. 5) suggesting the passing of high-density turbidity currents.

389 Cores KERO-01 and KERO-11 are within the sediment wave field on the northwest side of
390 the main channel (Figs. 5 and 7). Thin sand layers (1-5 cm), with maximum grain size ranging
391 from 100 to 350 μm , interbedded with clay comprise the first meter of KERO-01 (Fig. 5).
392 This succession overlies two meters of bioturbated clay (alternation of light and dark brown
393 clay layers) interstratified with sandy layers (1 or 2 cm thick) and silty laminae. The light
394 brown clay is dominated by calcareous sediment (nannoplankton and foraminifera), while the
395 dark brown clay mainly contains siliceous organisms (radiolarians and diatoms). Between
396 3.06 meters below seafloor (mbsf) and 3.17 mbsf, the core shows a normally graded sandy
397 interval with no visible structure, ranging from silty clay to coarse sand. The deepest part of
398 the core is composed of 73 cm of brown clay. In this core, thin fine sand layers are interpreted
399 as fine-grained turbidite deposits. The thickest sandy layer (11 cm thick) is interpreted as a
400 coarse turbidite deposit. The location of the core in the sediment wave field and the types of
401 deposits (thin sandy layers) suggest that these deposits were emplaced by overflow of a high
402 density turbidity currents

403 KERO-11 is mostly composed of sand (Figs. 5 and 11). The top of the core shows a 1 m thick
404 sandy layer (grain size between 150 and 200 μm) that is normally graded (Fig. 11). The base
405 of the layer is structureless and is overlain by an interval with horizontal laminations
406 (foraminifera-rich laminae including bathyal foraminifers) (Fig. 11). A second 30 cm thick
407 normally graded sandy layer (grain size between 100 and 200 μm) is present in the lower part
408 of the core at about 1.75 mbsf. These two layer are composed of the Ta and Tb division of the
409 Bouma sequence (Bouma, 1962). These sandy layers are interpreted as high-density turbidite
410 deposits. Based on grain size, we have calculated a sand/mud ratio of about 95:5.

411 In this upper part of the Cilaos turbidite system, the Kullenberg corer failed to recover in three
412 locations, one in the canyon area and two in the proximal fan, suggesting clean sand layer
413 (Fig. 2).

414

415 **4.3.2. Sedimentary facies in the distal fan**

416 In the distal fan, sediments are finer than in the proximal fan except for core KERO-13 (Fig.
417 5). A change in sedimentary facies and successions is observed between the western part and
418 the central part.

419 KERO-16 (4.95 m long) and KERO-17 (5.34 m long) are located in the central part of the
420 Cilaos turbidite system (Fig. 10). KERO-16 is located on the northwest side of the channel
421 and KERO-17 is from the channel floor (Figs. 10 and 9).

422 The first 1.4 meters of KERO-16 are characterized by silty layers (grain size between 50 and
423 100 μm) thinner than 1 cm interbedded with muddy hemipelagic intervals. The base of silty
424 layers is composed of laminated intervals. Muddy intervals are bioturbated and contain
425 foraminifera. Two AMS date were obtained in these muddy intervals at 0.6 m and 1.22 m
426 below sea floor (Table 2). They are dated respectively at 13.12 ka and 34.42 ka. These silty
427 deposits correspond to fine-grained turbidites with a sand/mud ratio of 20:80. The location of
428 the core on the channel edge and the succession of thin silty layers suggest that these deposits
429 are overflow deposits corresponding to unit U3, which is particularly thin on the channel side
430 (Fig. 9). Between 1.4 mbsf and 4.95 mbsf, the core is composed of clay layers (alternation of
431 light brown clay and darker brown clay) with bioturbation. This sedimentary facies correlates
432 with the semi-transparent unit U2 observed in the echosounder profiles (Fig. 9)

433 KERO-17 shows a succession of eight sandy and silty layers, interbedded with muddy
434 deposits. The thickness of silty and sandy layers varies from 1 cm in the lower part of the core
435 to 50 cm in the upper part and the grain size ranges from 50 to 150 μm (Figs. 5 and 9). The
436 upper first 75 cm of the core are composed of a thick normally graded sandy layer. The base
437 of the layer is structureless (Ta division of the Bouma sequence) and is overlain by an interval
438 with planar and cross laminations (Tb and Tc division of the Bouma sequence). Two other
439 sandy layers are visible over this thick unit at 0.8 and 1.15 mbsf (Fig. 11). Their thicknesses
440 are 8 and 15 cm respectively and they are characterized by planar and cross laminations (Fig.
441 11). These three units were interpreted as coarse-grained turbidite with a sand/mud ratio of
442 70:30. Between 1.30 and 5 mbsf four sandy units are interbedded with muddy deposits that
443 contained well preserved bathyal foraminifera. They are characterized by a thickness of about
444 5 cm and normally graded fine sand with cross laminations (Tc division of the Bouma
445 sequence). The clay layers are highly bioturbated with low foraminifera content. These
446 deposits correspond to fine grained turbidite deposits. The last sandy layer, at 5.05 m bsf, is
447 15 cm thick and composed of a basal structureless layer (Ta division of the Bouma sequence)
448 and is overlain by an interval with planar and cross laminations (Tb and Tc division of the
449 Bouma sequence). In the echosounder profiles, KERO-17 correlates with high-amplitude
450 reflectors (Fig. 9) typical of unit U3.

451 The two cores KERO-09 and KERO-15 are located on the northwest side of the main channel
452 of the western part of the study area, at about 215 km from the coast of the island for KERO-
453 09 and 280 km for KERO-15 (Fig. 10). They recovered to 6.27 m and 6.68 m of sediment
454 (Table 1) and show similar sedimentary successions to one another (Figs. 5 and 9). This
455 succession is characterized by a thick layer of clay in the top of cores (respectively 2 and 3 m
456 thick for KERO-09 and KERO-15) showing alternation between light brown clay and highly
457 bioturbated darker brown clay. Two AMS date were obtained in the light brown clay
458 (dominated by calcareous sediments) for core KERO-09 at 0.03 m and 0.69 mbsf (Table 2).
459 They are dated at 13.30 ka and 42.6 ka respectively (Table 2). This clay unit overlays a
460 succession of four sandy layers for KERO-09 and seven sandy layers for KERO-15 (grain
461 size between 50 and 150 μm). These sandy layers (about one sequence per meter) are 15-20
462 cm thick and up to 35 cm in KERO-15. They are composed of well-sorted fine sand with both
463 planar and cross laminations overlain by silty laminations and clay (Fig. 11). This succession
464 corresponded to Tb, Tc, Td and Te Bouma intervals (Bouma, 1962). In the dark sandy layers,
465 laminations are underlain by white laminae with a high content of foraminifera (Fig. 11).
466 These deposits are typical of low-density turbidites with a sand/mud ratio of 40:60 for core
467 KERO-09 and of 30:70 for KERO-15. The clay-rich interval correlates with the semi-
468 transparent unit U2 observed on echosounder profiles (Fig. 9) and the turbidite succession
469 corresponds to the stratified unit U1.

470 KERO-13 is located near core KERO-09, in the channel floor of the western part of the Cilaos
471 Fan (Fig. 10). It is composed of two units of massive sand, fine-grained sand in the upper part
472 and medium to coarse sand in the lower part of the section (small pebbles and high preserved
473 bathyal foraminifera) (Fig. 5). It is highly deformed by the coring process (Piston effect).
474 These deposits are interpreted as high density turbidity currents with a sand mud ratio of 95:5.

475

476 **5. Discussion**

477 **5.1. Sedimentary architecture of the Cilaos deep-sea fan**

478 The geographic partitioning of sediment accumulation allows the definition of two areas of
479 sedimentation.

480 - 1) The proximal fan, which corresponds to a wide area mainly composed of a few shallow
481 channels (Figs. 3 and 7) and characterized by relatively coarse-grained turbidites in the upper
482 depositional units of sediment core samples (Figs. 5 and 11).

483 - 2) The distal fan, characterized by a system of well-defined channels (Figs. 3 and 10), and
484 by fine-grained turbidites in lower depositional units of sediment core samples (Figs. 5 and
485 11).

486 The Cilaos turbidite system is classified as a sand rich system (Saint-Ange et al., 2011).
487 According to the model of sand-rich and point-source deep-sea fans established by Reading
488 and Richards (1994), a sand-rich submarine fan is moderate in size, tends to have a radial
489 shape, and is characterized by channelized lobes and unconfined channels without well-
490 developed levees. This setting is partly comparable with the proximal part of the Cilaos fan,
491 where an unconfined channel system with lobate structures is observed, while downslope it
492 evolves into a confined system with well incised channels as observed in the western and
493 central distal fan. Here, we suggest that the preexisting seafloor topography highly influenced
494 the morphology of the fan with the flow being confined among volcanic ridges. This favored
495 the development of small and well-incised channels, whose pattern was controlled by the
496 abyssal plain morphology in most part of the distal fan.

497 In the proximal fan, the turbidity current moved on relatively steep slope and had a high
498 content of coarse-grained sediment, as observed on core KERO-11 and KERO-17. Normark
499 and Piper (2001) suggest that coarse-grained turbidity currents tend to be faster and more
500 erosive than fine grained turbidity currents, especially if they are moving on relatively steep
501 slopes. So the lack of levee in the proximal fan can be explained by a strongly erosive
502 turbidity current enriched in coarse-grained sediment as observed in the Lagoa Parda oil field,
503 where most of the deep channels filled with coarse sediment do not have associated levees
504 (Bruhn and Walker, 1997). In the distal Cilaos fan, the percentage of sand decreases but
505 remains significant at about 40%, which explain the low development of the levees observed
506 on echosounder profiles FOR-45, Ero2-07, FOR-4a and FOR-4b (Fig. 8).

507 The complex geometry of the Cilaos fan is controlled by the steep submarine slopes of La
508 Réunion, the morphology of the basin, and by abundance of sediment supply (Saint-Ange et
509 al., 2011).

510 **5.2. Sediment source of turbidity currents**

511 Studies on the morphology of La Gomera Island or Tenerife Island, with a similar volcanic
512 context and drainage pattern, show that submarine canyons are often found off major river
513 mouths and are incised by turbidity currents (Krastel et al., 2001; Llanes et al., 2009; Mitchell
514 et al., 2003). Some turbidites reveal a high component of upper bathyal foraminifers

515 (Schneider et al., 1998) suggesting that clastic material was stored on the upper slope before it
516 was removed by turbidity current or was delivery directly from the subaerial fluvial system.
517 The high preservation of bathyal foraminifers and the location of canyons offshore major
518 river mouths suggest a hyperpycnal activity before the development of insular shelves that led
519 to the disconnection of the canyons from their fluvial sources (Mitchell et al., 2003). At La
520 Réunion, the large newly discovered turbidite systems are directly linked to the hydrographic
521 network and high preserved bathyal foraminifera are observed in the distal cores, suggesting a
522 climatic influence and the role of hyperpycnal processes in the generation of turbidity
523 currents. As proposed by Saint-Ange et al. (2011), the main source of sediment on the Cilaos
524 fan is the Rivière Saint-Etienne that feeds the system by hyperpycnal flows, but this detailed
525 study suggests that other processes can also occur.

526 The well-developed Pierrefonds canyon and the upper part of the Saint-Etienne canyon, that
527 show high reflectivity and smooth floor (Fig. 4), are connected to the coast by narrow
528 tributary canyons (Fig. 4) and not directly to the present river mouth as for the main Saint-
529 Etienne canyon head. This configuration suggests a contribution of sediment supply from
530 coastal processes to the canyon. The limited size and incision of gullies feeding the Saint-
531 Etienne canyon at the East of the “Etang-Salé” ridge (“Etang-Salé” beach) and the larger
532 extension of the insular shelf in this coastal sector are in good agreement with the existence of
533 coastal processes. Local slope instabilities triggered by waves can be invoked.

534 The high reflectivity visible in the Pierrefonds canyon and the Upper part of the Saint-Etienne
535 canyon and the coarse-grained deposits of core KERO-18 suggest the occurrence of coarse-
536 grained and high energy sediment flows. The large size and the mature morphology of the
537 Pierrefonds canyon can be explained by its location in front of the paleo-river outlet, which
538 supplied a large volume of sediment when the main river mouth was located in Pierrefonds.

539 The North Valley and the lower part of the Saint-Etienne canyon are different, with a rough
540 floor corresponding to a mottled appearance on the backscatter image. The rough seafloor can
541 be related to local instabilities (Le Friant et al. 2011; Oehler et al., 2008)). This instability
542 seems younger than the Saint-Etienne canyon because the chaotic deposits fill the lower
543 Saint-Etienne canyon (Fig. 4). The North Gullies and the narrow incision in the lower Saint-
544 Etienne canyon cut the chaotic deposits, indicating a recent feeding of the system by recurrent
545 flow processes generated from the hydrographic network.

546 In summary, the Cilaos turbidite system is fed by several types of sources: direct feeding by
547 the present river supply, local slope instabilities in the coastal area triggered by waves, and

548 local submarine events as demonstrated by chaotic deposits in the North Valley and in the
549 lower Saint-Etienne canyon.

550 **5.3. Model of Cilaos turbidite system growth**

551 Three depositional units are mapped in the Cilaos fan, based on the correlation between
552 echosounder profiles and cores. In the distal part, fine-grained turbidites showing cross-
553 bedded structures, visible on core KERO-15 and KERO-09, are linked to the stratified unit
554 U1 (Fig. 9). The thick clay layer, which covers these turbidites, is strongly correlated to the
555 transparent unit U2 (Fig. 9). The sandy turbidites, located in the upper part of core KERO-01,
556 KERO-11, KERO-16 and KERO-17 are linked to the stratified unit U3 (Fig. 9). These three
557 units were recognized over the entire fan using echosounder profiles. Some extract of
558 interpreted profiles across the three parts of the fan are shown in figure 9. Based on this
559 interpretation, three synthetic longitudinal sections showing the distribution of the three units
560 across the fan were developed (Fig. 9). This shows three stages in the construction of the
561 Cilaos fan.

562 The first stage (T1) (Fig. 12), corresponding to the unit U1, is characterized by long run out
563 turbidity currents that spread over the entire fan and which deposited sands that were 10-30
564 cm thick. These deposits are overlain by 2-3 m of hemipelagic mud. Using the AMS dates we
565 calculated a sedimentation rate for the two cores KERO-09 and KERO16 to estimate the age
566 of the top of unit U1. We obtained a sedimentation rate of 2.25 (KERO-09) and 2.9 cm /ka
567 (KERO-16) for the upper Pleistocene and the Holocene. These results are comparable to the
568 minimum sedimentation rate of 1.9 cm/ka proposed by Ollier et al. (1998) in this area during
569 the same period. Their results are based on micropaleontological analyses. Using a mean rate
570 of 2.5 cm/ka, we obtain an age of about 120 ka for the last turbidite observed on core KERO-
571 09 and an age of about 80 ka for the last turbidite observed on core KERO-15. The oldest
572 stage (U1) is characterized by intense turbidity current activity as demonstrated by the
573 succession of thick sandy turbidite in cores from distal location (more than 250 km from the
574 coast).

575 The second stage (T2) (Fig. 12) in the construction of the Cilaos fan corresponds to unit U2.
576 This layer is visible over the entire fan (Fig. 9), except for the more proximal parts. It is
577 characterized by a thick layer of hemipelagic mud, which we interpret as marking an
578 interruption of turbidity current activity. The limit of unit U2 is visible in core KERO-16. It is
579 the last sandy layer at 1.45 m from the top of core indicating the last turbidite of unit U3. The

580 estimate age of this limit is about 42 ka based on the AMS date of KERO-16 and the
581 sedimentation rate calculated for this core.

582 The third stage (T3) (Fig. 12), corresponding to the unit U3, represents the most recent
583 activity of the Cilaos fan. This unit is limited to the proximal fan and to a recent infilling of
584 the channels of the distal part, and corresponds to coarse-grained turbidites. On echosounder
585 profiles, most of the channels of the distal area are capped by the transparent unit U2 (Fig. 8,
586 profiles FOR-13 to FOR-4a), indicating that the channels are older than the recent turbidite
587 deposits belonging to unit U3. The recent turbidity current activity induced local reactivation
588 of channels with erosion of the hemipelagic drape (unit U2) and resulted in deposition of
589 turbidites.

590 The limit between the unit U3 and U2 can be correlated to the end of effusive activity of the
591 Piton des Neiges at about 30 ka (Gillot and Nativel, 1982), while the limit between unit U2
592 and U1, between 80 and 120 ka, can be correlated to highstand sea levels of the last
593 interglacial. At present, it remains difficult to establish whether the different stages in the
594 construction of the Cilaos fan are associated with the volcanic activity of La Reunion Island,
595 the cirques formation, or if they result from global climatic change of the late Quaternary as
596 suggested by Quidelleur et al (2008).

597

598 **5.4. Flow type and dynamics**

599 As demonstrated, the recent activity of the Cilaos turbidite system includes canyons, the
600 proximal fan and part of the channels of the distal fan. Sandy layers dominate the sedimentary
601 facies. The proximal fan is a radial-shaped fan with a diameter of 100 to 150 km. Only few
602 structures are observed in this part of the fan; mainly a braided system of unconfined channels
603 in the western part and lobe complexes. These characteristics suggest that density currents are
604 sand-rich with high energy during their flow into the canyon where the slope angles range
605 from 8° on the upper slope to 1° at 4000 m water depth (Fig. 5). They probably reach the base
606 of the slope with a relative high velocity and have the ability to flow and transport coarse
607 sediment (sand) over more than 100 km. The available cores for the proximal fan are not
608 located in the main flow axis and provide an approximation of the grain-size distribution
609 there, likely relatively coarse sand.

610 The field of sediment-waves observed in the upper part of the proximal fan is explained by a
611 change in flow dynamic of the density currents, probably due to the occurrence of a slope

612 break (corresponding to the base of the volcanic edifice) (Fig. 5). Upslope migration, different
613 asymmetrical shapes and lack of cross-bedding (Figs. 5 and 11) suggest that this field of
614 sediment-waves was cyclic (Cartigny et al., 2011). The change in dynamics could correspond
615 to a hydraulic jump implying the expansion of the flow volume, the increase of flow
616 turbulence and the rapid decrease of the flow velocity (Garcia and Parker, 1989; Garcia, 1993;
617 Piper and Normark, 2001). This change could induce the deposition of extended lobes without
618 the incision of a deep channel and the development of sandy sediment waves at the “channel-
619 lobe” transition as described in other turbidite systems (Morris et al., 1998; Wynn et al., 2002;
620 Wynn and Stow, 2002).

621 Analyses of the Cilaos deep-sea fan shows that the distal fan is marked by older turbidity
622 current activity characterized by extensive turbidite deposits (Unit U1) and possible
623 synchronous incision of channels over 300 km from the island. The turbidity currents
624 producing these sedimentary bodies probably had characteristics quite different from the
625 recent turbidity flows. Unlike the proximal fan, the old turbidite activity of the distal fan
626 shows fine grained deposits composed of very fine sands and silts (U1 in the core KERO-09
627 and KERO-15). These deposits are quite different from the coarse-grained turbidites of core
628 KERO-13, corresponding to the recent activity of the distal fan. The presence of structures
629 suggesting levee deposits on the channel sides (as shown on echosounder profiles) combined
630 with the extensive channel system is in good agreement with a lower density and a higher
631 mud content of the flow compared to the most recent turbidites (Unit U3). All these
632 characteristics suggest a system with a more efficient sediment transport, probably more
633 comparable to a mixed system (mud/sand). Throughout the past activity of the Cilaos
634 turbidite fan, we suggest that the sediment source could have been quite different than the
635 present sediment source, either with a higher contribution of hemipelagic sediment
636 (reworking of the submarine slope) or higher mud content in the island erosion products (in
637 relation with different chemical weathering and possible climate variation).

638 **6. Conclusions**

639 Five volcanoclastic turbidite systems were identified off La Réunion Island. The Cilaos deep-
640 sea fan constitutes a complex turbidite system, over 250 km long, that involves large amount
641 of sediment. New high-resolution multibeam and subbottom data and piston cores allow the
642 first accurate sedimentary characterization of this volcanoclastic system. The Cilaos deep-sea
643 fan is connected to the coast through two major canyons linked to the Rivière Saint-Etienne,
644 which supplies sand derived from the Piton des Neiges volcano. These canyons fed a fan

645 divided into a lobate proximal fan and a channelized distal fan. The architecture of the fan
646 appears atypical because of a preexisting seafloor topography that has clearly influenced
647 depositional processes during the edification of the deep-sea volcanoclastic fan.

648 A detailed study of the canyons allows the identification of several processes feeding turbidity
649 currents. In addition to a direct feeding by the river with the generation of hyperpycnal flows
650 as observed in other works, a feeding by local instabilities is also observed. Slope instabilities
651 are occurring along the coast and the slope of the volcano, which are able to bring significant
652 sediment volumes in an oceanic basin adjacent to a volcano.

653 The recent Cilaos fan was constructed in three stages. A first stage, older than 80 ka, a second
654 step between 42 and 80 ka, characterized by an interruption of the turbidite activity and a
655 third stage, younger than 42 ka, corresponding to the recent turbidite activity mainly in the
656 proximal fan.

657 The Cilaos fan can be defined as a unique sand-rich turbidite system showing an atypical
658 large extent. The study of such a turbidite system illustrates the importance of the marine
659 volcanoclastic sedimentation, too often underestimated in the studies of volcanic island
660 evolution.

661

662 **Acknowledgments**

663 This paper is dedicated to Bruno Savoye (1961-2009), geologist and geophysicist at
664 IFREMER, who had initiated this research project offshore La Réunion Island. The authors
665 thank the crew and scientific teams for the high-quality data recovery during the 2006
666 FOREVER cruise aboard the R/V *L'Atalante*, the 2006 ERODER1 cruise aboard the BHO
667 *Beautemps-Beaupré*, and the 2008 ERODER 2 cruise aboard the RV *Meteor*. Financial
668 support was provided by the “Conseil Régional de La Réunion” and by IFREMER. Internal
669 reviews by David Mosher and Robbie Bernnett helped clarify our ideas and writing. The
670 authors thank Dr. Claudia Romagnoli, an anonymous reviewer, and Editor David J.W. Piper
671 whose comments and suggestions contributed to improve the original manuscript.

672

673 **References**

674 Acosta, J., Uchupi, E., Munoz, A., Herranz, P., Palomo, C., Ballesteros, M., Grp, Z.E.E.W.,
675 2003. Geologic evolution of the Canarian Islands of Lanzarote, Fuerteventura, Gran

676 Canaria and La Gomera and comparison of landslides at these islands with those at
677 Tenerife, La Palma and El Hierro. *Marine Geophysical Researches* 24, 1-40
678 Arnaud, N., 2005. Les processus de demantelement des volcans, le cas d'un volcan bouclier
679 en milieu oceanique : le Piton des Neiges (Ile de La Réunion). Université de La Réunion,
680 France, pp. 422
681 Bachelery, P., Chevallier, L., Gratier, J.P., 1983. Structural characteristics of historical
682 eruptions of the Piton de la Fournaise (Reunion Island). *Comptes Rendus De l'Academie*
683 *Des Sciences Serie II* 296, 1345-1350
684 Barcelo, A., Robert, R., Coudray, J., 1997. A major rainfall event: The 27 February 5 March
685 1993 rains on the southeastern slope of Piton de la Fournaise massif (Reunion Island,
686 southwest Indian Ocean). *Monthly Weather Review* 125, 3341-3346
687 Bonneville, A., Barriot, J.P., Bayer, R., 1988. Evidence from geoid data of a hotspot origin
688 for the southern Mascarene Plateau and Mascarene Islands (Indian Ocean). *Journal of*
689 *Geophysical Research* 93, 4199-4212
690 Bosman, A., Chiocci, F.L., Romagnoli, C., 2009. Morpho-structural setting of Stromboli
691 volcano revealed by high-resolution bathymetry and backscatter data of its submarine
692 portions. *Bulletin of Volcanology* 71, 1007-1019
693 Bouma, A.H., 1962. Sedimentology of some flysch deposits: a graphic approach to facies
694 interpretation. Elsevier, Amsterdam 168 pp
695 Bret, L., Fevre, Y., Join, J.L., Robineau, B., Bachelery, P., 2003. Deposits related to
696 degradation processes on Piton des Neiges volcano (Reunion Island): overview and
697 geological hazard. *Journal of Volcanology and Geothermal Research* 123, 25-41
698 Bruhn, C.H.L., Walker, R.G., 1997. Internal architecture and sedimentary evolution of coarse-
699 grained, turbidite channel-levee complexes, Early Eocene Regência Canyon, Espírito
700 Santo Basin, Brazil. *Sedimentology* 44, 17-46
701 Cartigny, M.J.B., Postma, G., van den Berg., J., Mastbergen, D.R., 2011. a comparative study
702 of sediment waves and cyclic steps based on geometries internal structures and numerical
703 modeling. *Marine geology* 280, 40-56
704 Casalbore, D., Romagnoli, C., Chiocci, F., Frezza, V., 2010. Morpho-sedimentary
705 characteristics of the volcanoclastic apron around Stromboli volcano (Italy). *Marine*
706 *Geology* 269, 132-148
707 Courtilot, V., Davaille, A., Besse, J., Stock, J., 2003. Three distinct types of hotspots in the
708 Earth's mantle. *Earth and Planetary Science Letters* 205, 295-308
709 De Voogd, B., Palome, S.P., Hirn, A., Charvis, P., Gallart, J., Rousset, D., Danobeitia, J.,
710 Perroud, H., 1999. Vertical movements and material transport during hotspot activity:
711 Seismic reflection profiling offshore La Reunion. *Journal of Geophysical Research-Solid*
712 *Earth* 104, 2855-2874
713 Deniel, C., Kieffer, G., Lecointre, J., 1992. New Th-230-U-238 and C-14 age determinations
714 from Piton des Neiges volcano, Reunion-A revised chronology for the Differentiated
715 Series *Journal of Volcanology and Geothermal Research* 51, 253-267
716 Deplus, C., de Voogd, B., Dymont, J., Bissessur, D., Sisavath, E., Depuiset, F., Mercier, M.,
717 2009. New insights on the oceanic lithosphere at La Reunion hotspot volcano, EGU
718 *Geophysical Research Abstracts* 11-5728, Vienna.
719 Deplus, C., Le Friant, A., Boudon, G., Komorowski, J.-C., Villemant, B., Harford, C.,
720 Segoufin, J., Cheminee, J.-L., 2001. Submarine evidence for large-scale debris
721 avalanches in the Lesser Antilles Arc. *Earth and Planetary Science Letters* 192, 145-157
722 Deptuck, M.E., Piper, D.J.W., Savoye, B., Gervais, A., 2008. Dimensions and architecture of
723 late Pleistocene submarine lobes off the northern margin of East Corsica. *Sedimentology*
724 55, 869-898

725 Duncan, R.A., Backman, J., Peterson, L., 1989. Reunion hotspot activity through tertiary
726 time: initial results from the Ocean Drilling Program, leg 115. *Journal of Volcanology*
727 *and Geothermal Research* 4, 193-198

728 Fèvre, Y., 2005. Mécanismes et vitesses d'érosion à l'échelle géologique sur une île
729 volcanique jeune à relief élevé - La Réunion (Océan Indien). Université de la Réunion,
730 France, pp. 217

731 Gailler, L.S., Lenat, J.F., Lambert, M., Levieux, G., Villeneuve, N., Froger, J.L., 2009.
732 Gravity structure of Piton de la Fournaise volcano and inferred mass transfer during the
733 2007 crisis. *Journal of Volcanology and Geothermal Research* 184, 31-48

734 Garcia, M., Parker, G., 1989. Experiments on hydraulic jumps in turbidity currents near a
735 canyon-fan transition. *Science* 245, 393-396

736 Garcia, M.H., 1993. Hydraulic Jumps in Sediment-Driven Bottom Currents. *Journal of*
737 *Hydraulic Engineering* 119, 1094-1117

738 Garcia, M.O., Hull, D.M., 1994. Turbidites from giant Hawaiian landslides-results from
739 Ocean Drilling Program site-842. *Geology* 22, 159-162

740 Garcin, M., Poisson, B., Pouget, R., 2005. High rates of geomorphological processes in a
741 tropical area: the Remparts River case study (Reunion Island, Indian Ocean).
742 *Geomorphology* 67, 335-350

743 Gervais, A., Savoye, B., Mulder, T., Gonthier, E., 2006. Sandy modern turbidite lobes: A new
744 insight from high resolution seismic data. *Marine and Petroleum Geology* 23, 485-502

745 Gillot, P.Y., Nativel, P., 1982. K-Ar chronology of the ultimate activity of Piton des Neiges
746 volcano Réunion Island, Indian Ocean. *Journal of Volcanology and Geothermal Research*
747 13, 131-146

748 Gillot, P.Y., Nativel, P., 1989. Eruptive history of the Piton de la Fournaise volcano, Réunion
749 Island, Indian Ocean. *Journal of Volcanology and Geothermal Research* 36, 53-65

750 Krastel, S., Schmincke, H.U., Jacobs, C.L., 2001. Formation of submarine canyons on the
751 flanks of the Canary Islands. *Geo-Marine Letters* 20, 160-167

752 Le Friant, A., Boudon, G., Arnulf, A., Roberson, R.E.A., 2009. Debris avalanche deposits
753 offshore St. Vincent (west indies): Impact of flank-collapse events on the morphological
754 evolution of the island. *Journal of Volcanology and Geothermal Research* 179, 1-10

755 Le Friant, A., Harford, C., Deplus, C., Boudon, G., Sparks, S., Herd, R., Komorowski, J.-C.,
756 2004. Geomorphological evolution of Montserrat (West Indies): importance of flank
757 collapse and erosional processes. *Journal of Geological Society London* 161, 147-160

758 Le Friant, A., Lebas, E., Clément, V., Boudon, G., Deplus, C., de Voogd, B., Bachélery, P.,
759 2011. A new model for the evolution of La Réunion volcanic complex from complete
760 marine geophysical surveys. *Geophysical Research Letter* 38, 10.1029/2011GL047489

761 Lenat, J.F., Boivin, P., Deniel, C., Gillot, P.Y., Bachelery, P., Fournaise, T., 2009. Age and
762 nature of deposits on the submarine flanks of Piton de la Fournaise (Reunion Island).
763 *Journal of Volcanology and Geothermal Research* 184, 199-207

764 Lenat, J.F., Labazuy, P., 1990. Morphologies et structures sous-marines de La Réunion.

765 Llanes, P., Herrera, R., Gómez, M., Muñoz, A., Acosta, J., Uchupi, E., Smith, D., 2009.
766 Geological evolution of the volcanic island La Gomera, Canary Islands, from analysis of
767 its geomorphology. *Marine Geology* 264, 123-139

768 Louvat, P., Allegre, C.J., 1997. Present denudation rates on the island of Reunion determined
769 by river geochemistry: Basalt weathering and mass budget between chemical and
770 mechanical erosions. *Geochimica et Cosmochimica Acta* 61, 3645-3669

771 Malengreau, B., Lenat, J.F., Froger, J.L., 1999. Structure of Reunion Island (Indian Ocean)
772 inferred from the interpretation of gravity anomalies. *Journal of Volcanology and*
773 *Geothermal Research* 88, 131-146

774 Masson, D.G., Watts, A.B., Gee, M.J.R., Urgeles, R., Mitchell, N.C., Le Bas, T.P., Canals,
775 M., 2002. Slope failures on the flanks of the western Canary Islands. *Earth-Science*
776 *Reviews* 57, 1-35

777 McDougall, I., 1971. The geochronology and evolution of the young volcanic island of
778 Réunion, Indian Ocean. *Geochimica et Cosmochimica Acta* 35, 261-288

779 Michon, L., Saint-Ange, F., 2008. Morphology of Piton de la Fournaise basaltic shield
780 volcano (La Reunion Island): Characterization and implication in the volcano evolution.
781 *Journal of Geophysical Research-Solid Earth* 113, B03203.10.1029/2005JB004118

782 Migeon, S., Weber, O., Faugères, J.-C., Saint-Paul, J., 1999. SCOPIX: A new X-ray imaging
783 system for core analysis. *Geo-Mar. Lett.* 18, 251-255

784 Mitchell, N.C., Dade, W.B., Masson, D.G., 2003. Erosion of the submarine flanks of the
785 Canary Islands. *Journal of Geophysical Research-Earth Surface* 108, F1-
786 6002.10.1029/2002JF000003

787 Moore, J.G., Clague, D.A., Holcomb, R.T., Lipman, P.W., Normark, W.R., Torresan, M.E.,
788 1989. Prodigious Submarine Landslides on the Hawaiian Ridge. *Journal of Geophysical*
789 *Research* 94, 17. 465-484

790 Morgan, W.J., 1981. Hot spot tracks and the opening of the Atlantic and Indian Oceans, The
791 Sea.

792 Morris, S.A., Kenyon, N.H., Limonov, A.F., Alexander, J., 1998. Downstream changes of
793 large-scale bedforms in turbidites around th Valencia channel mouth, north-west
794 Mediterranean: implications for paleoflow reconstruction. *Sedimentology* 45, 365-377

795 Normark, W.R., Piper, D.J.W., 1991. Initiation processes and flow evolution of turbidity
796 currents: implications for depositional record, in Osborne, R.H. (Ed), *From Shoreline to*
797 *Abyss: Contribution in LMarine Geology in Honor of Francis Parker Shepard*. SEPM
798 *Special Publication* 46, 207-230

799 Oehler, J.-F., Lénat, J.-F., Labazuy, P., 2008. Growth and collapse of the Reunion Island
800 volcanoes. *Bulletin of Volcanology* 70, 717-742

801 Oehler, J.F., de Vries, B.V., Labazuy, P., 2005. Landslides and spreading of oceanic hot-spot
802 and arc shield volcanoes on Low Strength Layers (LSLs): an analogue modeling
803 approach. *Journal of Volcanology and Geothermal Research* 144, 169-189

804 Oehler, J.F., Labazuy, P., Lenat, J.F., 2004. Recurrence of major flank landslides during the
805 last 2-Ma-history of Reunion Island. *Bulletin of Volcanology* 66, 585-598

806 Ollier, G., Cochonat, P., Lenat, J.F., Labazuy, P., 1998. Deep-sea volcanoclastic sedimentary
807 systems: an example from La Fournaise volcano, Reunion Island, Indian Ocean.
808 *Sedimentology* 45, 293-330

809 Peltier, A., Famin, V., Bachelery, P., Cayol, V., Fukushima, Y., Staudacher, T., 2008. Cyclic
810 magma storages and transfers at Piton de La Fournaise volcano (La Reunion hotspot)
811 inferred from deformation and geochemical data. *Earth and Planetary Science Letters*
812 270, 180-188

813 Peltier, A., Staudacher, T., Bachelery, P., Cayol, V., 2009. Formation of the April 2007
814 caldera collapse at Piton de La Fournaise volcano: Insights from GPS data. *Journal of*
815 *Volcanology and Geothermal Research* 184, 152-163

816 Piper, D.J.W., Normark, W.R., 2001. Sandy Fans - From Amazon to Hueneme and Beyond.
817 *AAPG Bulletin* 85, 1407-1438

818 Quidelleur, X., Hildenbrand, A., Samper, A., 2008. Causal link between Quaternary
819 paleoclimatic changes and volcanic islands evolution. *Geophysical Research Letters* 35,
820 L02303.10.1029/2007GL031849

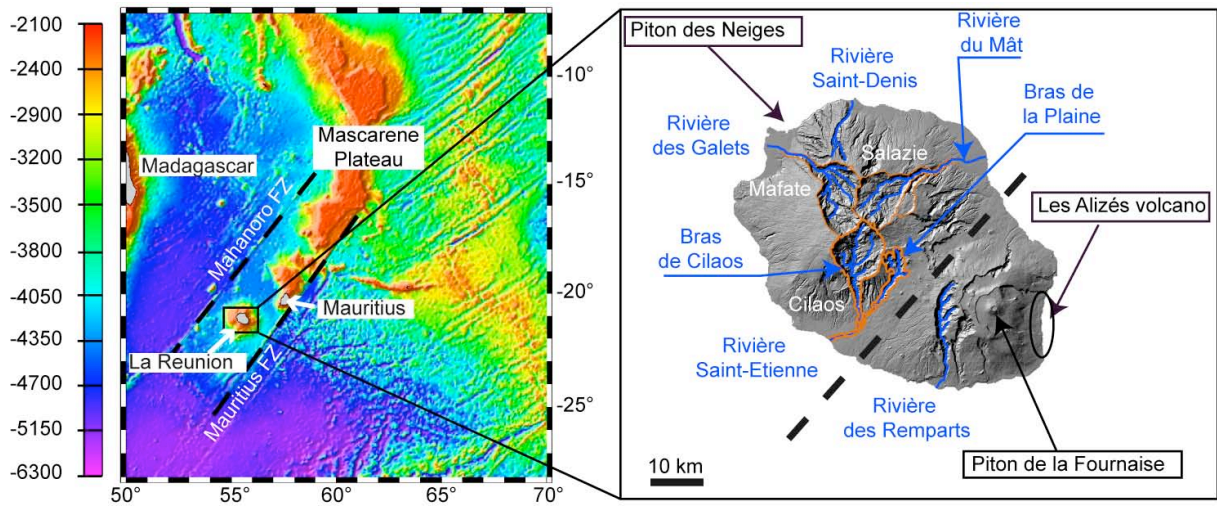
821 Quidelleur, X., Holt, J.W., Salvany, T., Bouquerel, H., 2010. New K-Ar ages from La
822 Montagne massif, Reunion Island (Indian Ocean), supporting two geomagnetic events in
823 the time period 2,2-2,0 Ma. *Geophysical Journal International* 182, 699-710

- 824 Rad, S.D., Allegre, C.J., Louvat, P., 2007. Hidden erosion on volcanic islands. Earth and
825 Planetary Science Letters 262, 109-124
- 826 Rancon, J.P., Lerebour, P., Auge, T., 1989. The Grand Brule Exploration Drilling - New Data
827 on the Deep Framework of the Piton-De-La-Fournaise Volcano .1. Lithostratigraphic
828 Units and Volcanostructural Implications. Journal of Volcanology and Geothermal
829 Research 36, 113-127
- 830 Reading, H.G., Richards, M., 1994. Turbidite Systems in Deep-Water Basin Margins
831 Classified by Grain-Size and Feeder System. AAPG Bulletin 78, 792-822
- 832 Reimer, P.J., Reimer, R.W., 2001. A marine reservoir correction database and on-line
833 interface. Radiocarbon 43, 461-463
- 834 Robert, R., 2001. Pluviométrie à l'île de La Réunion: des travaux de J. Defos du Rau (1960) à
835 nos jours. L'information géographique N°1, 53-59
- 836 Romagnoli, C., Kokelaar, P., Casalbore, D., Chiocci, F.L., 2009. Lateral collapses and active
837 sedimentary processes on the northwestern flank of Stromboli volcano, Italy. Marine
838 Geology 265, 101-119
- 839 Rousset, D., Lesquer, A., Bonneville, A., Lenat, J.F., 1989. Complet gravity study of Piton de
840 la Fournaise volcano, Reunion Island. Journal of Volcanology and Geothermal Research
841 36, 37-52
- 842 Saint-Ange, F., 2009. La sédimentation volcanoclastique en contexte de point chaud (île de La
843 Réunion, Océan Indien). PhD Université de La Réunion, France, pp. 279
- 844 Saint-Ange, F., Piper, D., Savoye, B., Michon, L., Deplus, C., Bachélery, P., de Voogd, B.,
845 Dymont, J., Le Drezen, E., Voisset, M., Le Friant, A., Boudon, G., 2011. A volcanoclastic
846 deep-sea fan off La Réunion Island (Indian Ocean): gradualism versus catastrophism.
847 Geology 39, 271-274
- 848 Sisavath, E., Saint-Ange, F., Babonneau, N., Bachelery, P., Deplus, C., de Voogd, B., Savoye,
849 B., 2009. Giant turbidite systems off La Réunion Island - Indian Ocean, EGU 2009.
850 Geophysical Research Abstracts 11: 7105 Vienna.
- 851 Smietana, M., Bachélery, P., Hémond, C., 2010. Heterogeneity in the Mantle Source of La
852 Réunion Island, Goldschmidt 2010. Geochimica et Cosmochimica acta 74 (12 Suppl. 1):
853 A972.
- 854 Smith, W.H.F., Sandwell, D.T., 1997. Global sea floor topography from satellite altimetry
855 and ship depth soundings. Science 277, 1956-1962
- 856 Société Grenobloise d'Etudes et d'Application Hydrauliques (SOGREAH), 1998. Etude des
857 risques Hydrauliques sur la Rivière Saint-Etienne. Société Grenobloise d'Etudes et
858 d'Application Hydrauliques report 554509 R1, 24 p
- 859 Stieltjes, L., Moutou, P., 1988. A statistical and probabilistic study of the historic activity of
860 Piton de la Fournaise, Reunion Island, Indian Ocean. Journal of Volcanology and
861 Geothermal Research 36, 67-86
- 862 Wynn, R.B., Kenyon, N.H., Masson, D.G., Stow, D.A.V., Weaver, P.E., 2002.
863 Characterization and recognition of deep-water channel-lobe transition zones. AAPG
864 Bulletin 86, 1441-1462
- 865 Wynn, R.B., Masson, D.G., Stow, D.A.V., Weaver, P.P.E., 2000. Turbidity current sediment
866 waves on the submarine slopes of the western Canary Islands. Marine Geology 163, 185-
867 198
- 868 Wynn, R.B., Stow, D.A.V., 2002. Classification and characterisation of deep-water sediment
869 waves. Marine Geology 192, 7-22

870
871
872
873
874

875 **Figures :**

876



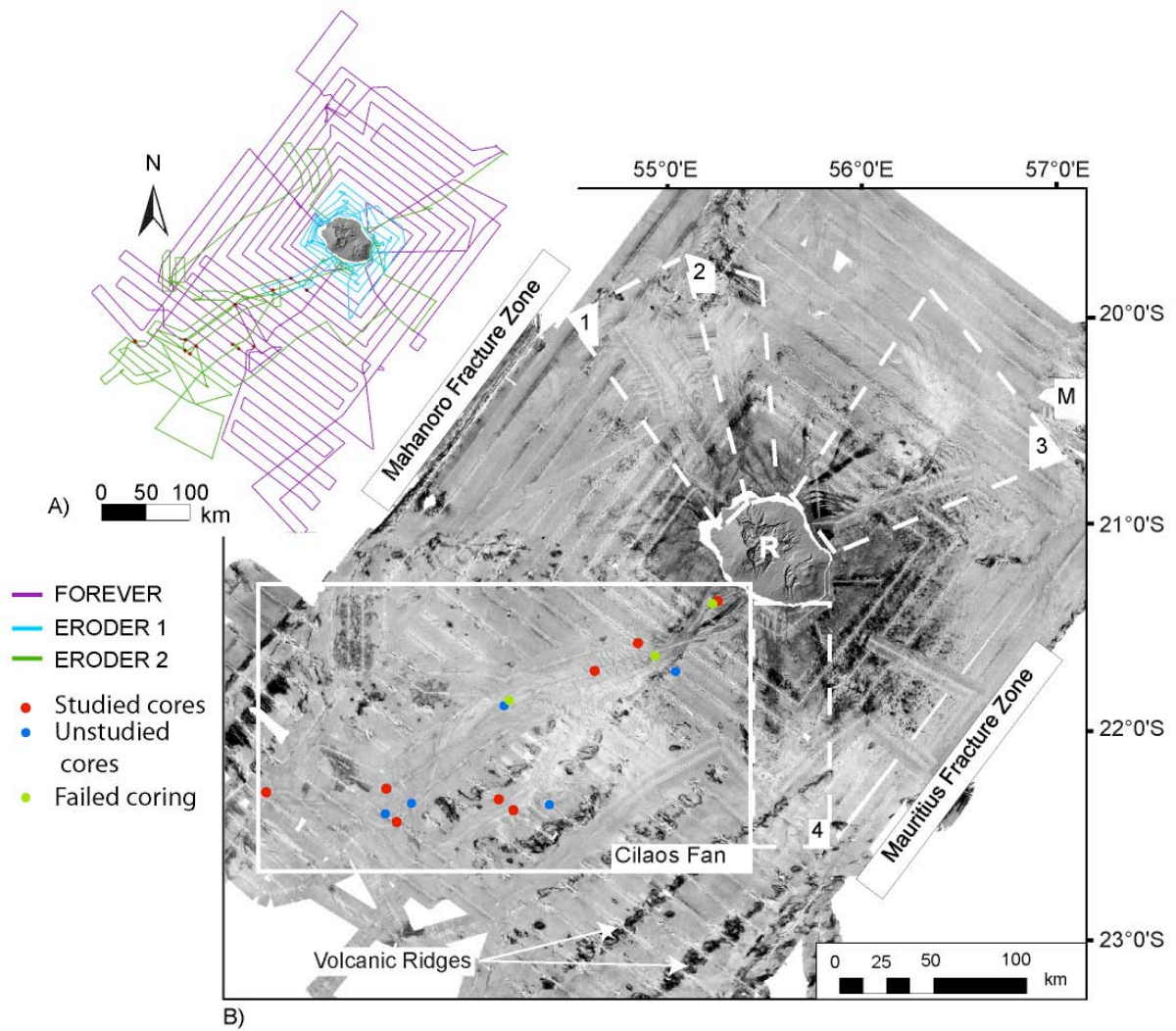
877

878

879 Fig. 1: Predicted bathymetry from Smith and Sandwell (1997) around La Réunion and
880 Mascarene plateau. Overview of the main geological structures of La Réunion Island (insert).

881 The dotted line represents the separation between the two main volcanic edifices.

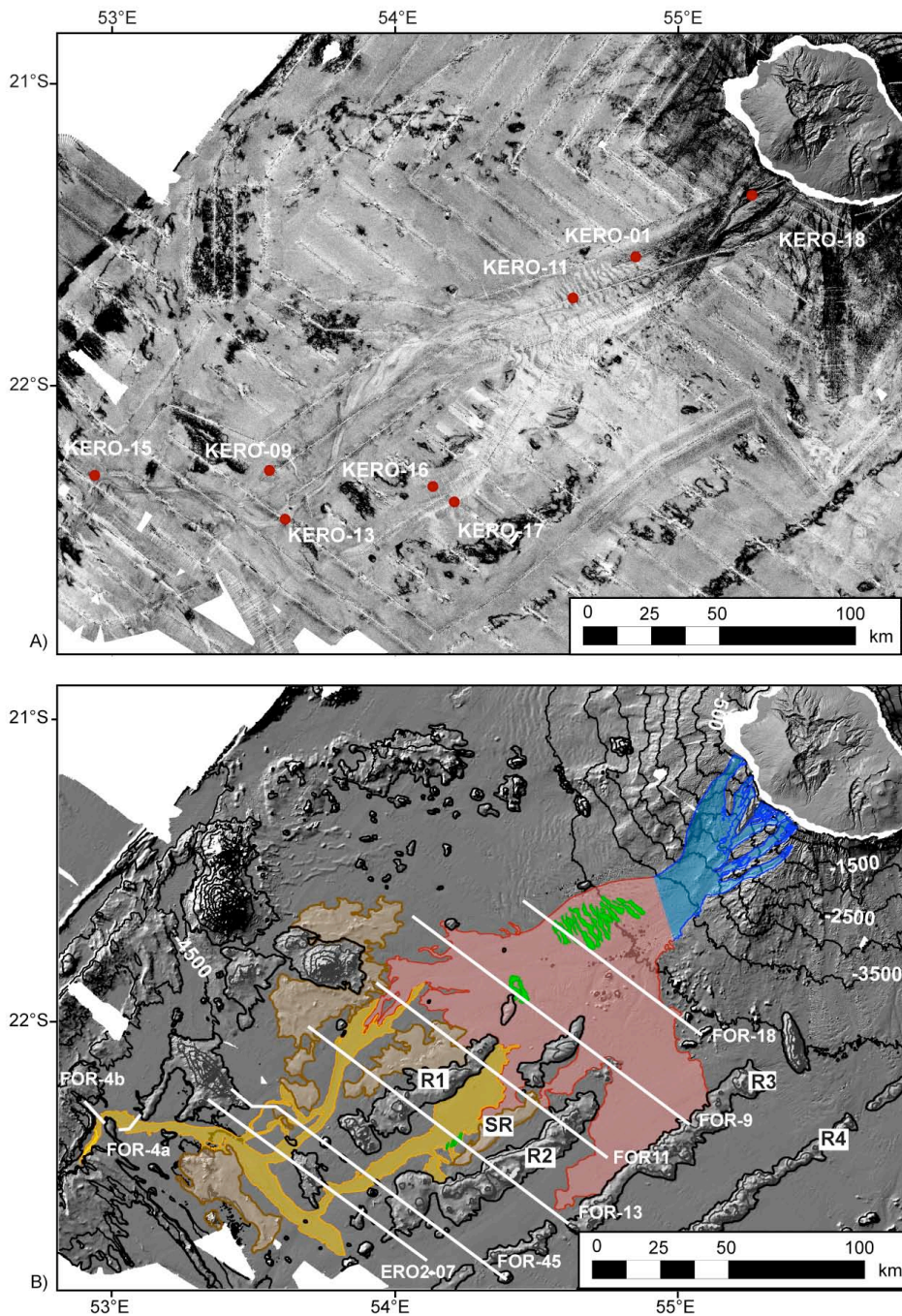
882



883

884

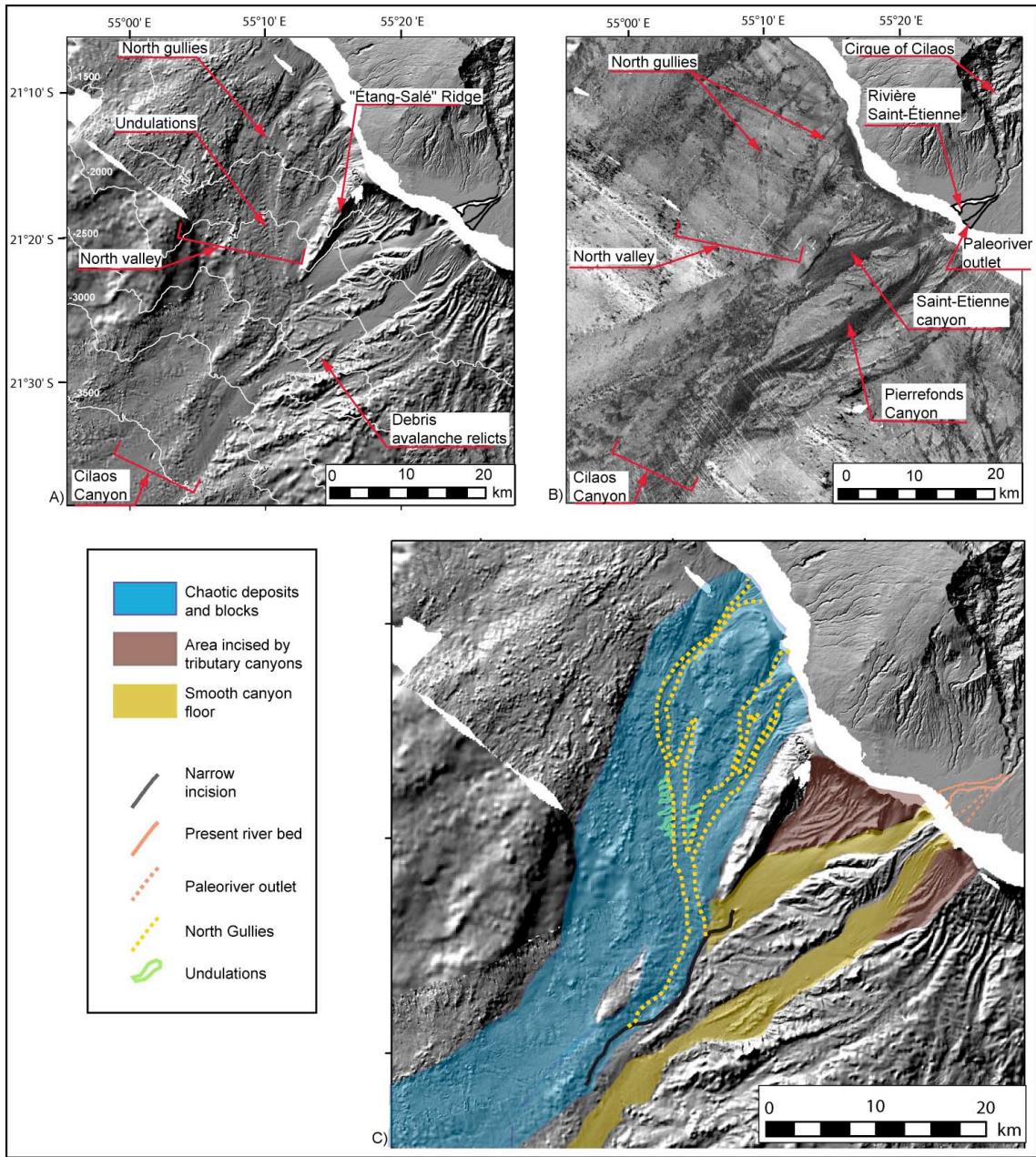
885 Fig. 2: A) Ship tracks of the three cruises FOREVER (purple line), ERODER1 (blue line) and
 886 ERODER2 (green line). B) Backscatter map compiled from ERODER and FOREVER
 887 surveys. White lines correspond to the location of the five fans discovered off La Réunion
 888 island: the Cilaos fan, the Mafate fan (1), the Saint-Denis fan (2), the Salazie fan (3) and the
 889 Saint-Joseph fan (4). Red dots correspond to sediment cores retrieved in the Cilaos turbidite
 890 system.



891

892

893 Fig. 3: A) Acoustic backscatter image (based on the FOREVER and ERODER data) of the
 894 southwest part of La Réunion showing details of the Cilaos fan. B) Interpreted shaded relief
 895 image of the southwestern flank of La Réunion, compiled from ERODER and FOREVER
 896 surveys, showing interpreted subdivisions of the Cilaos fan and the location of Parasound and
 897 3.5 kHz echosounder profiles of figure 8. Canyons are in blue, the proximal fan is outlined in
 898 red, the distal fan in yellow, volcanic highs in dark grey, sediment reliefs in light brown, and
 899 sediment waves in green.



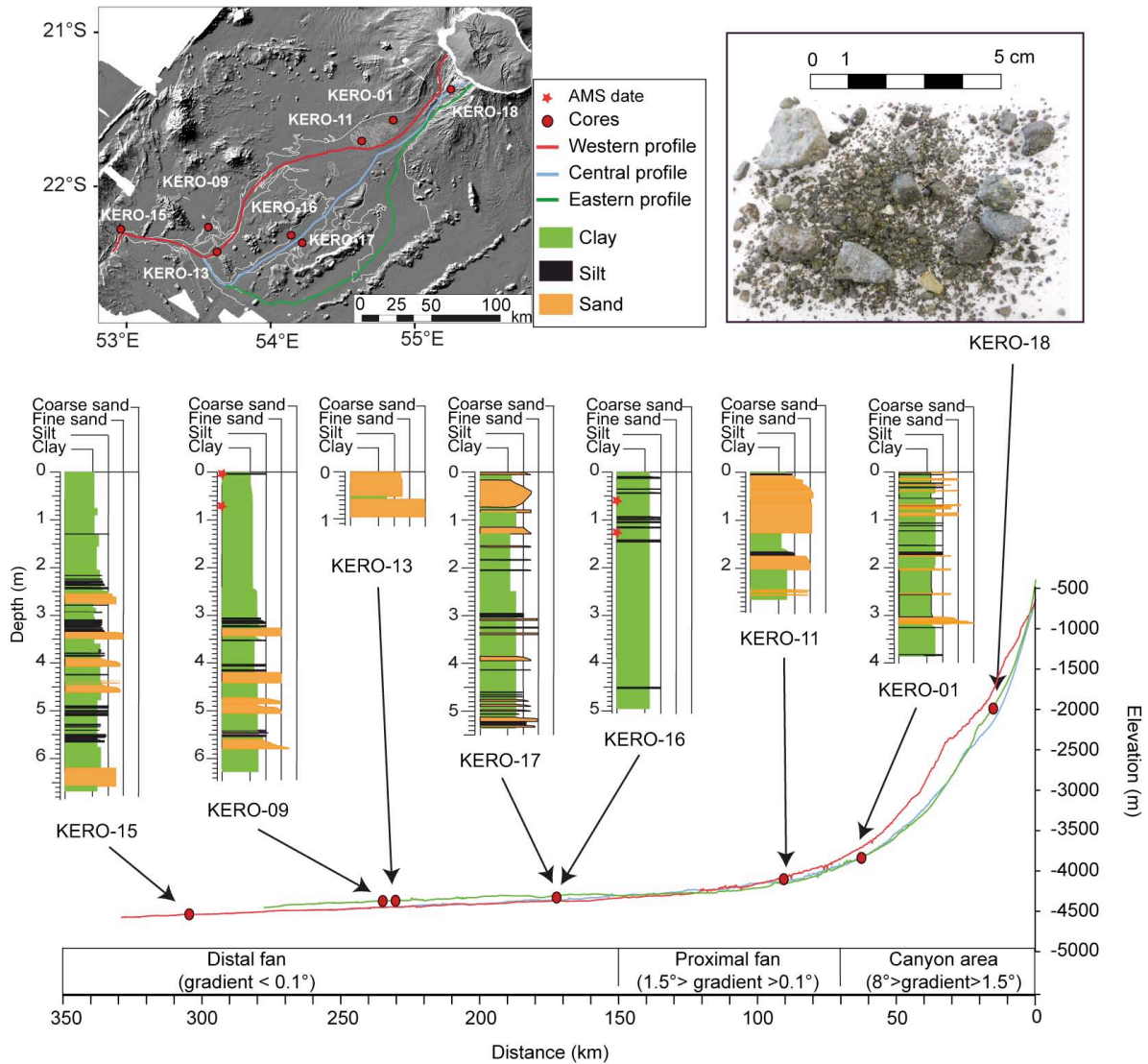
901

902

903 Fig. 4: (A) Swath shaded bathymetry and (B) backscatter image of the canyons area of the
 904 Cilaos turbidite system; (C) interpreted image of the canyons area.

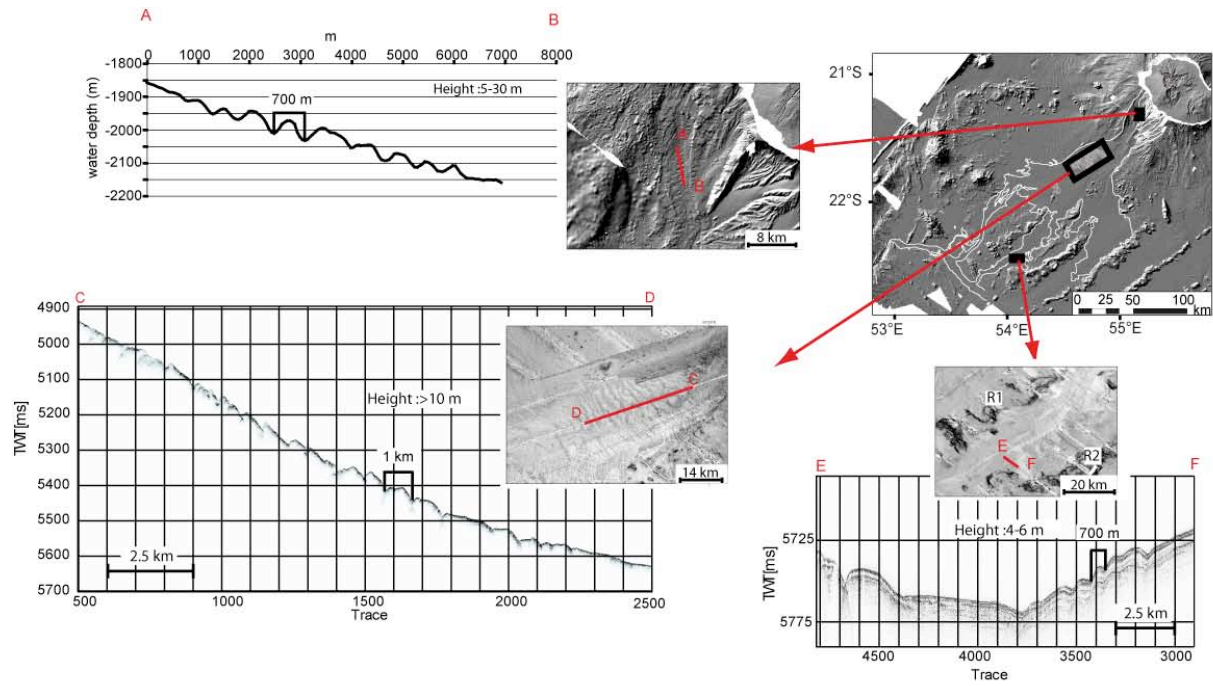
905

906



907
 908
 909
 910
 911
 912

Fig. 5: Slope gradient map with the location of the studied cores. A lithologic log is illustrated for each core, except KERO-18 where only 30 cm of coarse-grained sands and gravels were collected.



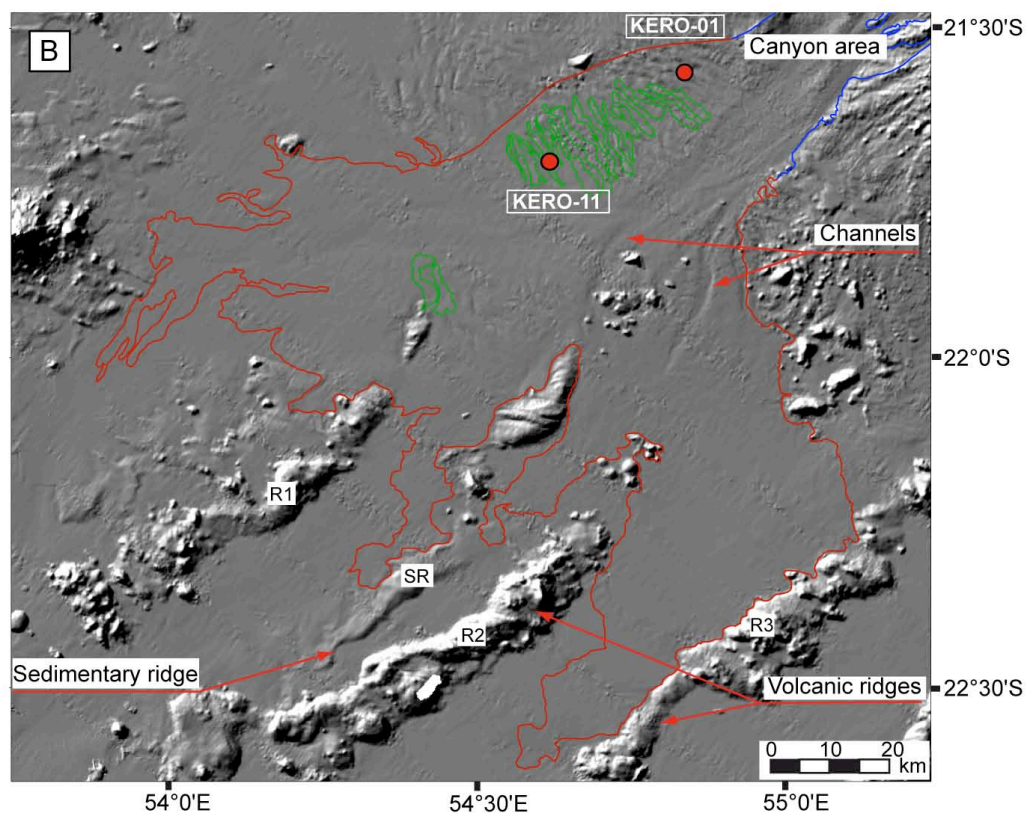
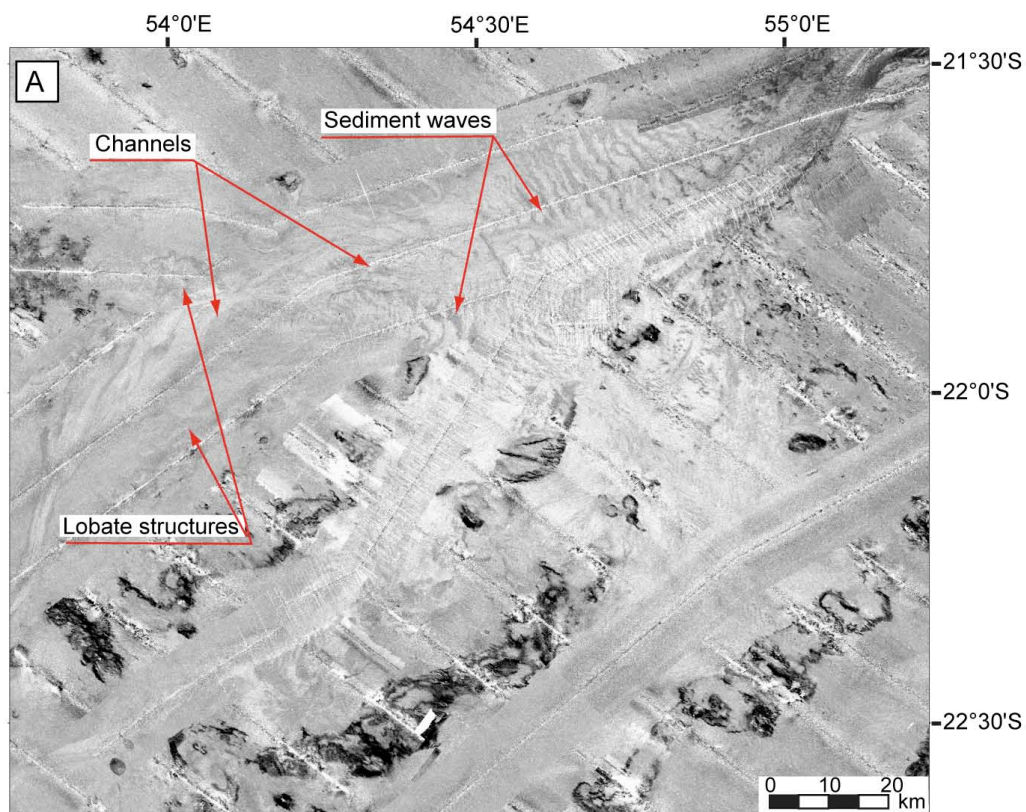
913

914

915 Fig. 6: Location of the three sediment wave fields observed in the Cilaos turbidite system.

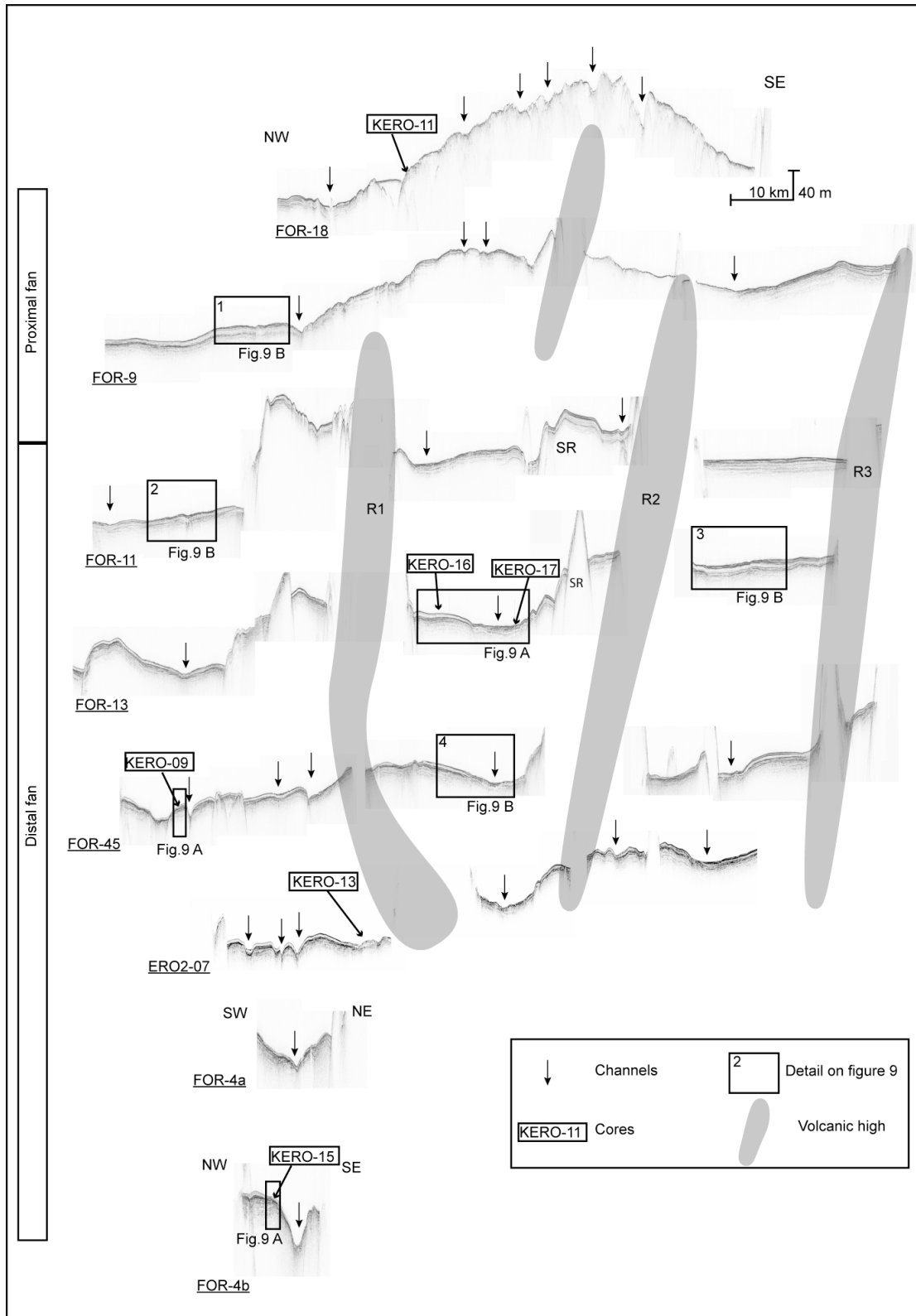
916 Profile A-B is topographic profile, profiles C-D and E-F are echosounder profiles.

917



918
919

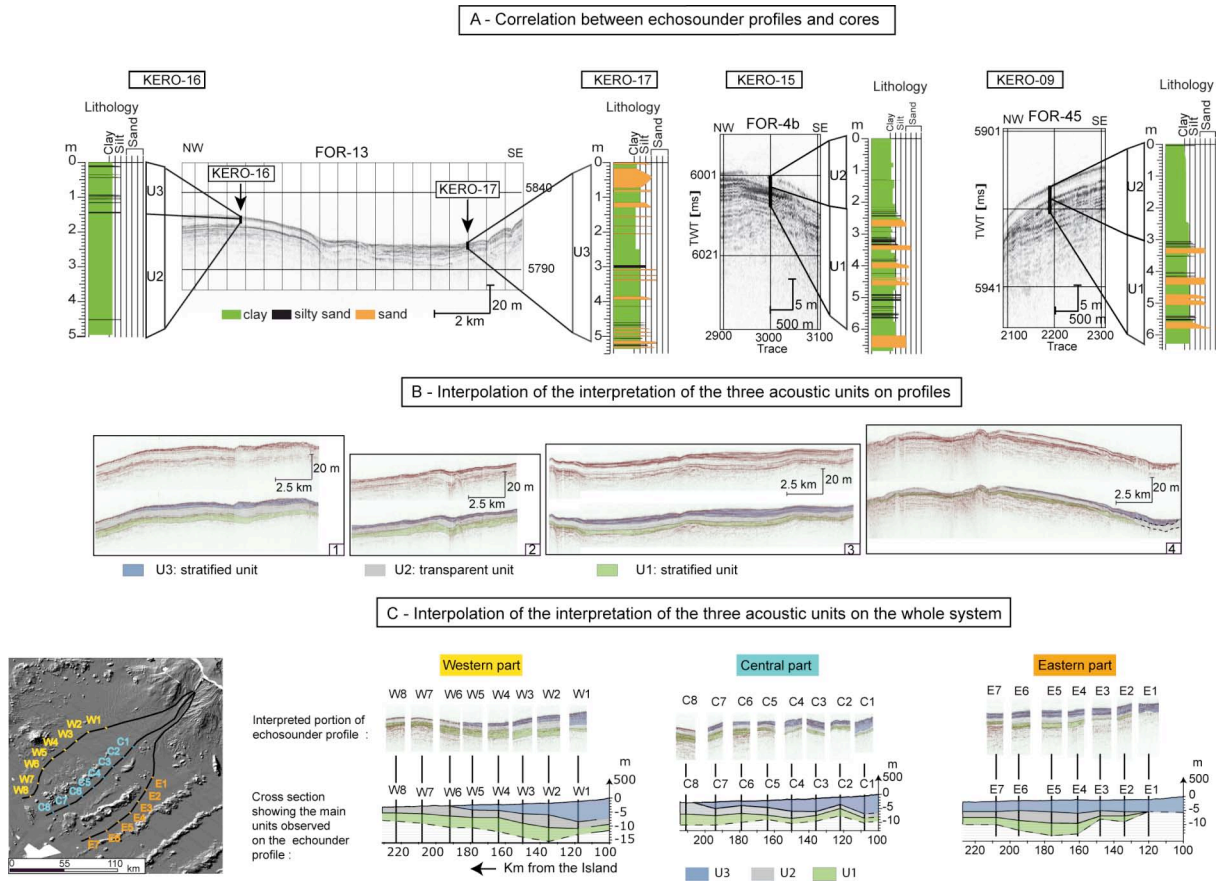
920 Fig. 7: (A) Backscatter image and (B) interpreted swath shaded bathymetry of the proximal
921 fan of the Cilaos turbidite system. Red filled dots correspond to sediment cores presented in
922 this paper.



923

924

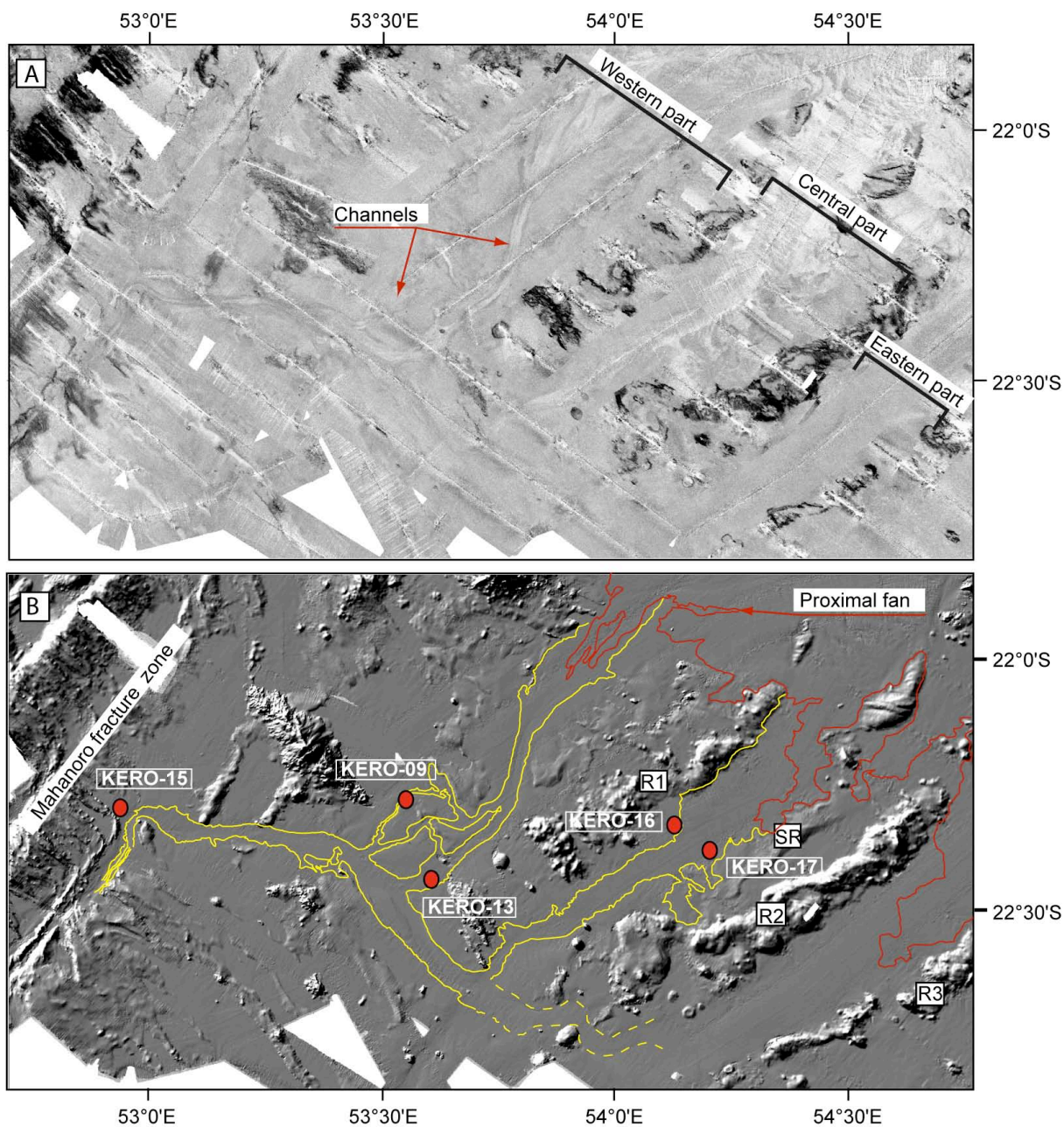
925 Fig. 8: Parasound and 3.5 kHz echosounder profiles showing the downstream evolution of the
 926 fan (Profile location in Fig. 3). All these profiles are NW-SE oriented except the SW-NE
 927 profile FOR-4a. Grey areas represent the location of volcanic ridges R1, R2, R3 intercepting
 928 the profiles.



930

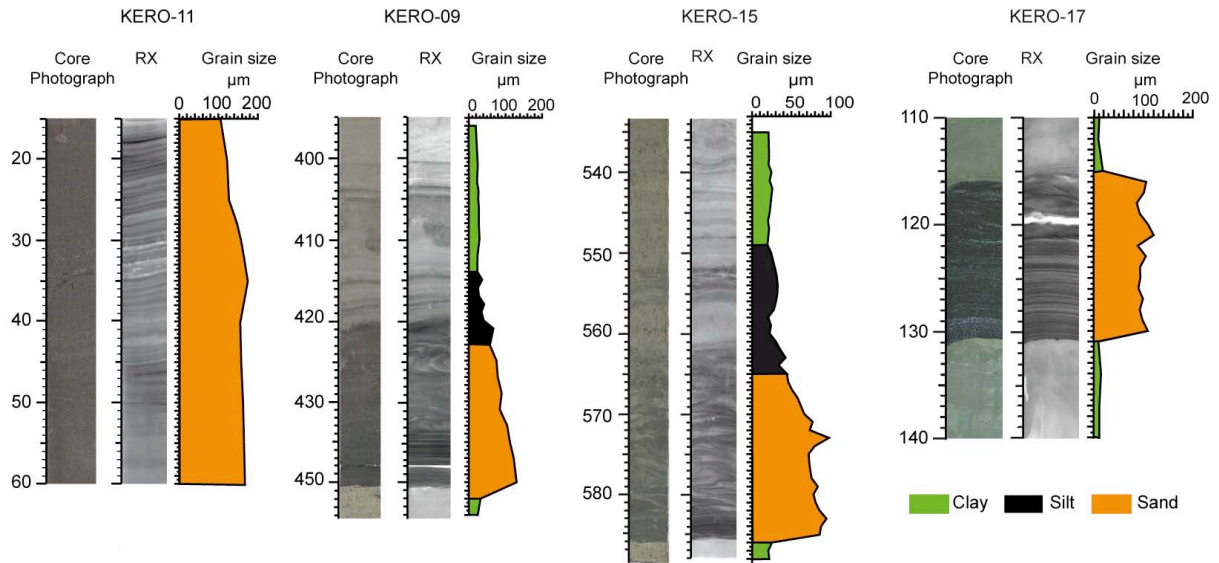
931

932 Fig. 9: A) Lithological logs correlated with corresponding echosounder profile; B) Non-
 933 interpreted and interpreted 3.5 kHz echosounder profiles, showing the succession of the three
 934 units U1 (in green), U2 (in grey) and U3 (in blue). For location of each profile see figure 8
 935 (black square). C) Interpretation of the three units U1 (in green), U2 (in grey) and U3 (in
 936 blue) on short portion of echosounder profiles, through the three parts of the fan.



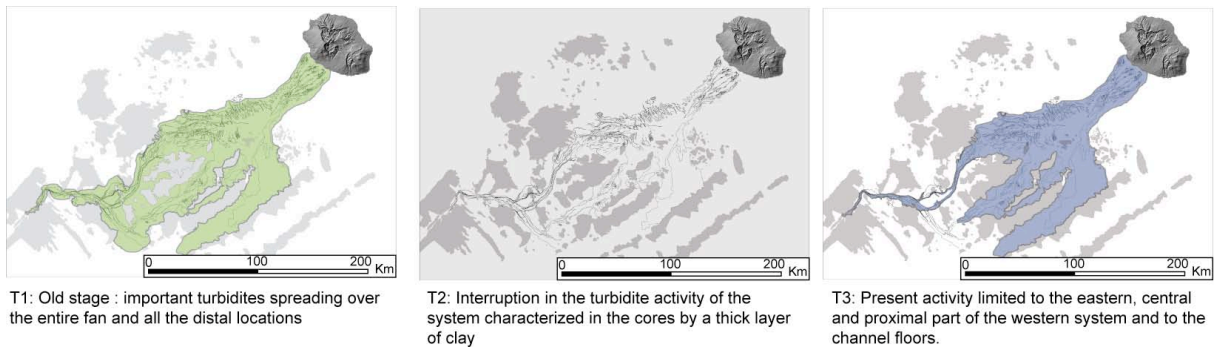
937
 938
 939
 940
 941
 942

Fig. 10: (A) Backscatter image and (B) interpreted swath shaded bathymetry of the distal fan of the Cilaos turbidite system. Red filled dots correspond to sediment cores presented in this paper.



943
944
945
946
947
948

Fig. 11. Grain size diagram, photograph, and X-ray image of few standard turbidite beds of cores KERO-11, KERO-09, KERO-15 and KERO-17.



949
950
951

Fig. 12. Schematic diagram illustrating the construction of the Cilaos turbidite system.

Cruises	Name and Core Type	Lat (S)	Long (E)	Water Depth (m)	Location	Length (m)
FOREVER	FOR-C1	S22°20.95	E54°23.33	4074	Sedimentary ridge, Central part of the distal fan	4.51
	FOR-C2	S21°52.347	E54°09.39	4346	Channel floor, Occidental proximal fan	5,52
ERODER 1	KERO-01	S21°50.902	E54°11.00	3816	Sediment Wave, Up. Cilaos fan	3,90
	KERO-03	S21°38.00	E54°56.00	3786	Channel floor, Occidental proximal fan	0
	KERO-02	S21°42.31	E54°37.29	3546	Channel floor, Up. Cilaos Fan	3,60
ERODER 2	KERO-09	S22°16.347	E53°33.060	4460	Channel side, western part of the distal fan	6.27
	KERO-10	S21°50.902	E54°11.00	4346	Channel floor of the Occidental proximal fan	0
	KERO-11	S21°42.31	E54°37.29	4164	Sediment Wave, Up. Cilaos Fan	2.65
	KERO-12	S22°23.550	E53°32.752	4461	Channel side, western part of the distal fan	6.40
	KERO-13	S22°25.98	E53°36.36	4407	Channel floor, western part of the distal fan	0.98
	KERO-14	S22°20.50	E53°40.88	4439	Channel floor, western part of the distal fan	3.47
	KERO-15	S22°17.39	E52°56.10	4529	Distal part, Cilaos distal fan	6.68
	KERO-16	S22°19.51	E54°07.78	4340	Channel side, Central part of the distal fan	4.95
	KERO-17	S22°22.540	E54°12.267	4353	Channel floor, Central part of the distal fan	5.34
	KERO-18	S21°22.00	E55°15.22	2056	Canyon area	Sample (~0,3)
	KERO-19	S21°22.873	E55°13.669	2221	Canyon area	0

953

954 Table 1: List of piston cores sampling the Cilaos turbidite system; names are in bold for cores
955 used in this paper.

956

Laboratory number	Core	Depth (cm bsf)	AMS 14C age (yr)	AMS 14C age (-400yr)	Error yr	Calendar Age (cal yr BP)
Poz-35177	KERO-09	3	11 840	11 440	60	13 302
Poz-35180	KERO-09	69	38 500	38 100	600	42 587
SacA 21882	KERO-16	60,5	11 610	11 210	35	13 118
SacA 21883	KERO-16	122,5	29 660	29 260	160	34 422

957

958 Table 2 : Radiocarbon dates from cores KERO-09 and KERO-16